MicroRNA-338-3p as A Novel Therapeutic Target for Intervertebral Disc Degeneration

Hua Jiang
Guangxi Medical University First Affiliated Hospital
Abu Moro
Guangxi Medical University First Affiliated Hospital
Jiaqi Wang
Guangxi Medical University First Affiliated Hospital
Dihua Meng
Guangxi Medical University First Affiliated Hospital
Xinli Zhan
Guangxi Medical University First Affiliated Hospital
Di Chen
Rush University Medical Center
Qingjun Wei (gxspine@163.com)
Guangxi Medical University First Affiliated Hospital https://orcid.org/0000-0002-3062-0353

Research

Keywords: intervertebral disc degeneration, microRNA-338-3p, Mitogen-activated protein kinase, Sirtuin 6

Posted Date: November 10th, 2020

DOI: https://doi.org/10.21203/rs.3.rs-101234/v1

Version of Record: A version of this preprint was published at Experimental & Molecular Medicine on September 16th, 2021. See the published version at https://doi.org/10.1038/s12276-021-00662-3.

Abstract

Background: Recent studies have demonstrated the pivotal role played by microRNA (miRNA) in the etiopathogenesis of intervertebral disc degeneration (IDD). The aim of this current study is to investigate whether intra-discal delivery of miRNA can attenuate IDD development.

Results: miR-338-3p expression was significantly increased in the nucleus pulposus (NP) of patients with IDD. Moreover, there was a statistically significant positive correlation between the level of expression of miR-338-3p and the severity of IDD. Our functional studies showed that miR-338-3p significantly influenced the expression of extracellular matrix synthesis of genes, as well as the proliferation and apoptosis of NP cells. Mechanistically, miR-338-3p aggravated IDD progression by directly targeting SIRT6, a negative regulator of MAPK/ERK pathway. Intra-discal injection of antagomir-338-3p significantly decelerated IDD development in mice models.

Conclusions: miR-338-3p is identified as a mediator of IDD, and thus may be a promising target for rescuing IDD.

Introduction

Intervertebral disc degeneration (IDD; OMIM 603932), one of most common spine disorders, is characterized by the progressive loss of disc space, endplate sclerosis and low back pain (LBP).[1] It is among the main factors affecting quality of life and exacts a huge burden on the global health-care system.[2, 3] An intervertebral disc is composed of a central nucleus pulposus (NP) and an outer annulus fibrosus (AF). The NP is involved in maintaining the homeostasis of proteoglycan and type II collagen (Col II) in the extracellular matrix (ECM).[4] The hallmark of IDD is the degradation of proteoglycan in the NP, leading to decreased disc height and reduces biomechanical function.[5, 6] Clinically, IDD causes disc herniation and sciatica, which is associated with back pain and chronic disabilities. With regard to therapeutics, IDD presents with a complex feature of degenerative diseases. The conservative and surgical treatments have limited long-term effects in many IDD cases as these methods only target the clinical symptoms but not focus on the etiology of IDD.[7] Recent advancements in gene therapy have opened an avenue for the possible prevention of IDD development at transcription or post-transcriptional levels.[8–11] There is therefore the need for a more in-depth understanding of IDD, in order to aid the development of new therapeutic strategies.[12]

MicroRNAs (miRNAs), a group of endogenous noncoding RNAs, has emerged as key regulators in the development of skeletal pathophysiology.[13] Studies have reported that they bind to the 3’ untranslated region (3’ UTR) of target mRNAs, resulting in the modulation of gene expression.[14] Accumulating evidence have demonstrated that miRNAs acts as a central modulator in essential cellular processes such as cellular proliferation and apoptosis.[15, 16] Of note, dysregulation of miRNAs is has been reported to be related with various degeneration diseases in humans.[17–20] Differential expression patterns of miRNAs have been noted in the pathogenesis of IDD. Several miRNAs, such as miR-155, miR-

93, and miR-141, were significantly downregulated or upregulated in patients with IDD, and thus are identified as targets of IDD-associated genes expressions ranging from matrix-degrading enzymes to pro-inflammatory cytokines.[21–24] In the current study, we performed a comprehensive screening of 2,000 miRNAs in human NP tissue. The miRNA expression profiling identified miR-338-3p to be substantially increased in the NP of IDD tissues compared with control NP tissue. Moreover, miR-338-3p expression was positively correlated with the Pfirmman grade of IDD. Our functional studies revealed that miR-338-3p induced IDD by promoting the catabolism of NP cells and apoptosis/cell death via Sirtuin 6 (SIRT6)/Mitogen-activated protein kinase (MAPK)/ Extracellular regulated protein kinases (ERK) pathway. Our in vivo study on investigating the possible effects of intra-discal injection of miR-338-3p inhibitor in mice models revealed that there was a NP-protective effect. Thus, our findings, for the first time, provide crucial evidence that miR-338-3p holds promise as a possible valuable target for the prevention of IDD.

Results

Identification of differentially expressed miRNAs between IDD patients and normal controls

In order to investigate dysregulated miRNAs, we scanned the expression profile of miRNA based on microarray in human NP tissues (3 IDD patients *vs.* 3 normal controls). The microarray revealed approximately 600 differentially expressed miRNAs between the IDD and control patients (Fig. 1A). The results of the unsupervised clustering analysis of miRNAs are shown in the volcano plot (Fig. 1B) and heat map (Fig. 1C). We identified a total of 14 upregulated and 9 downregulated miRNAs that exhibited a mean fold change more than 5 fold or less than 0.2 fold as well as p-values less than 0.05. Specifically, miR-338-3p, miR-198, and miR-874-3p were found to be significantly dysregulated in the NP of IDD but not in that of the control (Supplementary Table 1). We performed qRT-PCR to identify the three top-ranked miRNAs based on a cohort of 110 patients with IDD and 103 normal controls. Among the top-ranked miRNAs, miR-338-3p was observed to be the most significantly upregulated in the NP tissues from IDD patients (Fig. 1D). Therefore, it was selected as the candidate miRNA for further studies. The qRT-PCR and fluorescence in situ hybridization (FISH) further confirmed miR-338-3p to be significantly increased in the NP of IDD patients when compared to that of the control (Fig. 1D, E). Our results also revealed the expression levels of miR-338-3p to be positively correlated with the Pfirmman grade of IDD ($n = 56$, $r = 0.855$, $P < 0.01$, Fig. 1F). In human NP cells, the expression levels of miR-338-3p were also found to be upregulated in IDD patients but not in normal controls (Fig. 1G).

The effect of miR-338-3p on proliferation and apoptosis of human NP cells

To determine the influence of miR-338-3p on the etiopathogenesis of IDD, we detected that the transfection with miR-338-3p mimics or inhibitor affected the cellular proliferation and apoptosis of human NP cells. The high transfection efficiency of miR-338-3p was confirmed by Cy3-labeled

fluorescence and qRT-PCR (Fig. 2A, B). At three different time periods (24 h, 48 h, and 72 h), the miR-338-3p inhibitor significantly activated cellular proliferation of NP cells, whereas the miR-338-3p mimics significantly repressed cellular proliferation of NP cells (Figure. 2C). Thus, in order to determine the effects of miR-338-3p on proliferation of NP cells, a 5-Ethynyl-2'-deoxyuridine (EdU) assay was undertaken (Fig. 2D). Correspondingly, the transfection of miR-338-3p mimics significantly promoted the apoptosis of NP cells (Fig. 2E). However, the silencing of miR-338-3p notably upregulated the expression of ECM related proteins (Col II and Aggrecan), whereas overexpression of miR-338-3p significantly enhanced expression of matrix-degrading enzymes (MMP9 and ADAMTS4) (Fig. 2F). These observations were further supported by immunofluorescence (Fig. 2G). Thus, our findings illustrate that the silencing of miR-338-3p could promote the proliferation of NP cells and enhance matrix synthesis.

SIRT6 as a target gene for miR-338-3p

Heat map was used to identify the dysregulated mRNAs in IDD (Fig. 3A). Gene ontology analysis predicted the functional characterization of downregulated gene including those involved in disc development, ECM structural constituency and extracellular region (Fig. 3B). Based on miRNA-mRNA network and Venn analysis, SIRT6 was identified as a target gene for miR-338-3p (Fig. 3C-E). Furthermore, the computational alignment scores indicated a high conservation of miR-338-3p among various animal species (Fig. 3F). The luciferase reporter assay confirmed that miR-338-3p mimics could inhibit luciferase activity of the wild-type SIRT6-3'UTR. Conversely, it failed to inhibit luciferase activity of the mutant-SIRT6-3'UTR (Fig. 3G). Our results thus indicate that miR-338-3p could directly bind to SIRT6 3'UTR, which suppress the expression levels of mRNA and protein of SIRT6 in human NP cells (Fig. 3H, I).

miR-338-3p regulates IDD by modulating SIRT6/MAPK/ERK signaling pathway

KEGG pathway analysis identified MAPK/ERK signaling pathway as the most significantly enriched pathways (Fig. 4A). Importantly, co-immunoprecipitation showed that SIRT6 could directly deacetylate the GRB2 that formed a key component of the upstream of MAPK/ERK signaling pathway (Fig. 4B, C). Thus we hypothesized that SIRT6 could inhibit the transactivation capacity of GRB2, leading to the suppression of MAPK/ERK pathway. The overexpression of miR-338-3p significantly increased MAPK/ERK signaling pathway-dependent protein (GRB2, p-ERK1/2), cellular senescence associated protein (P16), apoptosis associated protein (Bax, Caspase 3), ADAMTS4 and MMP9 activities (Fig. 4D). These effects were maintained upon SIRT6 silencing (Fig. 4D). We further validated the possible direct relationship between miR-338-3p and SIRT6 using the level of anabolic/catabolic markers such as Col II, Aggrecan, MMP9 and ADAMTS4 (Fig. 4E, F). Our results revealed that the inhibition of SIRT6 induced by miR-338-3p was able to trigger cellular senescence and apoptosis, thus promoting IDD via the MAPK/ERK pathway.

Intra-discal delivery of miR-338-3p inhibitor attenuates IDD development

Following the elucidation of the effect of miR-338-3p on the etiopathogenesis of IDD, in a first step towards translation, we sought to investigate its possible therapeutic effect on IDD mice model via intra-discal injection of miR-338-3p inhibitor. The therapeutic testing was performed via local injection of injury-induced IDD mice with miR-338-3p (antagomir-338-3p or agomir-338-3p) on the 1st, 7th, and 14th days postoperatively (Fig. 5A). Live imaging of mice was used to monitor the in vivo disc-targeted ability of antagomir-338-3p or agomir-338-3p, and Cy3-labelled analysis was used to confirm the efficiencycy of in vivo delivery of antagomir-338-3p or agomir-338-3p into intervertebral disc (Fig. 5B, C). According to radiographic evaluation[25], a higher percentage of disc height index (DHI) was observed in IDD mice treated with antagomir-338-3p (Fig. 5D). The intra-discal delivery of antagomir-338-3p significantly attenuated both cellular and morphological degeneration of AF and NP according to the modified histologic grading system[25–27] (Fig. 5E). These radiographic and histologic findings suggest that miR-338-3p silencing could exert a therapeutic influence on the development of IDD. On the contrary, the treatment of IDD mice with agomir-338-3p markedly aggravated disc degeneration. Immunofluorescence demonstrated analysis showed that administration of antagomiR-338-3p downregulated the expression of catabolic marker (MMP9) and upregulated the expression of anabolic marker (Col II) in NPs (Fig. 5F). This indicates that antagomiR-338-3p regulated the imbalance between degradation and synthesis of NPs. In line with the aforementioned findings, TUNEL staining was performed which further confirmed the significantly decreased level of cellular apoptosis in the NP cell of IDD mice model injected with antagomiR-338-3p (Fig. 5G). Thus, our findings indicate that the miR-338-3p inhibitor (antagomiR-338-3p) can be used as a potential therapeutic agent which could alleviate and reverse IDD.

Discussion

To the best of our knowledge, our study (both in vitro and in vivo) is the first to evidently reports on the possible functional role that can be played by miR-338-3p in the search for a viable therapeutic target for the treatment of IDD. In accordance with miRNA expression profiling, we detected the expression levels of miR-338-3p to be remarkably increased in degenerated human discs, which was further confirmed via qRT-PCR in an independent cohort. Notably, we found a noteworthy positive correlation between miR-338-3p expression and the severity of IDD. Thus, our results indicate the possible role miR-338-3p can play as a possible novel biomarker for the prognosis of IDD. Based on several computational tools, SIRT6 was determined to be the direct target of miR-338-3p. Furthermore, our results identified the expression levels of SIRT6 was downregulated in degenerated NPs, and that miR-338-3p could directly interact with SIRT6. Our findings also showed an inverse relation between miR-338-3p and SIRT6 and therefore demonstrate that both miR-338-3p and SIRT6 may be important mediators in the pathogenesis of IDD.

SIRT6 is a member of the sirtuin family of deacetylases which are involved in diverse pathologies including neurodegeneration, metabolic homeostasis, and aging.[28–30] The link between SIRT6 and MAPK signaling has been well reported in multiple systems. For instance, SIRT6 has been reported to protect against hepatic ischemia/reperfusion injury by regulating the transcriptional status of MAPK/ERK signaling-related genes.[31] Recent studies have provided evidence that implicates increased activation of MAPK signaling pathway promotes disc degeneration.[32–34] However, the possible functional role of

SIRT6 deacetylase activity in MAPK signaling pathway is yet to be fully understood. We hypothesize that SIRT6 may be involved in influencing the development of IDD through the MAPK signaling pathway and its deacetylase activity was essential in engaging this process. Our study is possibly the first to identify that SIRT6 could modulate MAPK/ERK signaling via transcriptional control of GRB2, which is an upstream activator of this signaling pathway. From the results of our co-immunoprecipitation study, we observed that the enhanced expression of GRB2 was likely the direct consequence of the deacetylating activity of SIRT6. Furthermore, our findings revealed that the upregulation of GRB2 expression in NP cells lead to significant increase in the expression of target proteins in the MAPK/ERK signaling (p-ERK1/2), as well as those involved in cellular senescence or apoptosis (P16, Bax, Caspase 3), ultimately resulting in the upregulation of the expression levels of MMP9 and ADAMTS4, and downregulation of expression of Col II and Aggrecan. The modulation of the MAPK signaling pathway by SIRT6 siRNA or miR-338-3p mimics is therefore possible via the regulation of GRB2 expression. Nevertheless, our findings do not exclude the possibility that other genes are involved in the control of MAPK/ERK signaling. There is therefore the need for a deeper exploration into the understanding of the mechanism by which miR-338-3p influence the expression of SIRT6 and GRB2 in future studies.

Our study provides a novel perspective for the clinical translation of miR-338-3p as a diagnostic and treatable option for IDD. The increased expression of miR-338-3p observed in IDD patients and animal models signifies that miR-338-3p can be used as a stable biomarker for this common musculoskeletal disease. Our in vitro study revealed that in the absence of miR-338-3p, the expression of SIRT6 was upregulated and MAPK/ERK signaling complex suppressed, resulting in reduced apoptosis of NP cells. Our results therefore indicate the viability of employing miR-338-3p as possible direct therapeutic target for rescuing the development of IDD. In our preclinical study, we found that antagomiR-338-3p (a miR-338-3p inhibitor) protected intervertebral disc against the typical pathological pattern of IDD, by inhibiting the apoptosis of NP cells, enhancing the expression of extracellular matrix proteins (Col II and Aggrecan) and inhibiting the expression of extracellular matrix-degrading enzymes (MMP9 and ADAMTS4). These findings suggest that the possible underlying therapeutic mechanism of miR-338-3p inhibition is via reversing the imbalance between catabolic and anabolic factors involved in IDD development. Collectively, our study introduces a new option of miR-338-3p-based therapeutics in IDD prevention. (Supplementary Fig. 1)

Conclusions

Our study revealed that miR-338-3p was significantly increased in humans with degenerative NP, and involved in the direct targeting of SIRT6, leading to the activation of MAPK/ERK signaling pathway in NP cells. Our results also revealed that antagomir-338-3p, a miR-338-3p inhibitor, could rescue IDD development. Thus miR-338-3p inhibitors can be used as possible novel agents for the therapeutic intervention of IDD.

Methods

Patient samples

Nucleus pulpous (NP) tissues were collected from 110 patients with intervertebral disc degeneration (IDD) who underwent lumbar microdiscectomy (mean age 56.3 ± 9.1 years). All IDD patients were clinically diagnosed by two qualified spine surgeons via physical examination and MRI. Based on their Pfirrmann classification[35], all patients were classified as mild/moderate degeneration (grades 1–2) or serious degeneration (grades 3 or 4). The normal NP tissues were collected from 103 patients with lumbar vertebral fracture who underwent anterior spine surgery (mean age 53.7 ± 4.6 years). These trauma patients had no prior history of preoperative low back pain or IDD.

This study was approved by the Ethics Committee of The First Affiliated Hospital of Guangxi Medical University (2018-KY-NSFC-025). All patients involved in the study gave signed consent for the use of their information and clinical condition in this study.

The injury-induced IDD model and therapeutic experiment

The injury-induced IDD mice model was established via needle puncture as previously described.[23, 36] Briefly, following general anesthesia of 12-week-old C57BL/6 mice, their coccygeal discs Co6/Co7 were exposed and then punctured with 31G syringe needle through the AF to NP. The needle was then left in the intervertebral disc at a depth of 1.5 mm for period of 10 seconds. The adjacent Co7/Co8 disc levels were not punctured as they were used as contrast segments.

For the therapeutic tests, 20 male mice that underwent the previously described injury-induced IDD surgery were randomly divided into 4 groups (n = 5): group 1 (agomir-control); group 2 (agomir-338-3p); group 3 (antagomir-control); and group 4 (antagomir-338-3p) (treatment group). The agomir- or antagomir-338-3p and their controls were acquired from RiboBio (RiboBio Co., Guangzhou, China). The injection mice with agomir-338-3p/agomir-control or antagomir-338-3p/antagomir- control were performed on the 1st, 7th, and 14th days post-needle puncture intervention. The disc samples were then harvested at two different time-periods: 6th week and 12th week post intervention.

The ethical committee of The First Affiliated Hospital of Guangxi Medical University approved the animal experimentation protocol, and all animal experimentations were conducted in accordance with the approved guidelines.

Cell culture

The human NP tissues were sliced into 1 mm^3 pieces and washed twice with 10% fetal bovine serum (PBS) (GIBCO, NY, USA), followed by incubation in DMEM (GIBCO, NY, USA). Subsequently, the resuspension of NP cells were cultured in DMEM, 1% penicillin-streptomycin and 10% FBS. The cells were then cultured in an incubator at 37 °C and 5% CO_2, and then dissociated with trypsin and split at a ratio of one to three.

Quantitative real-time polymerase chain reaction (qRT-PCR)

Trizol (Invitrogen Life Technologies, CA, USA) was used for total RNAs extraction. The RNA templates were then synthesized into cDNA using the iScripts cDNA Synthesis kit (Quanta Biosciences, MD, USA), and GAPDH used as control for normalization. The isolated miRNA were then quantified using qScript microRNA cDNA Synthesis Kit (Quanta BioSciences, MD, USA), with U6 snRNA used as the internal control. Thereafter, SYBR Green real-time PCR kit (Quanta Biosciences) was then used to perform the qRT-PCR, with comparative threshold cycle (△△Ct) adopted for the calculation of gene expression. The specific primers are listed in Supplementary Table 2.

miRNA microarrays and miRNA target prediction

The miRNA microarray was conducted using Affymetrix® 4.0 miRNA Array (USA). Total RNAs were obtained from six individual NP samples with or without IDD. Based on volcano plot and fold change filtering, we identified the differentially expressed miRNAs in IDD. Candidate miRNAs were identified if they met the following criteria: (1) exhibited more than 5 fold changes or less than 0.2 fold changes; (2) p-values less than 0.05. Gene Cluster software (Stanford University) and DAVID software were used for hierarchical cluster analysis and functional group analysis respectively. TargetScanHuman (www.targetscan.org/) and microRNA.org were used to forecast the miRNA target genes and to analyze mRNA binding sites.

miR-338-3p and SIRT6 transfection

For overexpression or silence of miR-338-3p, human NP cells were transfected with miR-338-3p mimics or inhibitors or their negative controls (Cat. No: 4464061 and 4464079, Life Technologies) using the Lipofectamine RNAiMAX Transfection Reagent (Invitrogen). For the suppression of SIRT6 expression, transient transfection of human NP cells with SIRT6 siRNA or control siRNA (Cat. No: 116148 and 4459408, Thermo Fisher Scientific) were carried out using Lipofectamine 3000 Transfection Reagent (Invitrogen). The SIRT6 expression plasmid (pcDNA3.1(+)/SIRT6) was obtained from Invitrogen.

Luciferase constructs and reporter assay

SIRT6 mRNA 3'UTR fragments including the binding sites of wild-type (wt) and mutant (mut) miR-338-3p, were inserted into the psiCHECK-2 luciferase reporter vector (Promega, WI, USA). A miR-338-3p expression plasmid or a control plasmid was then co-transfected with SIRT6 wt- or mut-3'UTR and their respective control plasmids into human NP cells. All Luciferase assays were conducted using Dual-Glo Luciferase Assay System (Promega, WI, USA), and luciferase activity measured by a fluorescence microplate reader (BioTek, USA).

Flow cytometry, Cell Counting Kit-8 (CCK8) and EdU assay

Cellular apoptosis was measured using apoptosis kit with Annexin V-FITC/PI (Cat. No: V13242, Invitrogen), and analysis performed with Beckman Coulter EPICS Altra (USA). The detection of cellular proliferation was performed using CCK8 (Dojindo Laboratories, Kumamoto, Japan). Human NP cells that received different transfections (miR-338-3p mimics, control mimics, miR-338-3p inhibitor or control inhibitor) were then collected into 96-well plates, and then cultured for 24, 48, and 72 h. Afterwards, CCK8

was added to incubate the cultured cells for 3 h, with absorption evaluated at 450 nm. The degree of cellular proliferation was then assessed using EdU assay. The human NP cells were incubated with EdU medium (Sigma-Aldrich, MO, USA), and the collected cells stained with Hoechst 33258.

Fluorescence in situ hybridization (FISH)

For the analysis of human NP using FISH, digoxin-labeled miR-338-3p probes with locked nucleic acid modifications were designed and synthesized using Exiqon- QIAGEN (Hilden, Germany). The fluorescence signals were detected using the FISH Kit (Exiqon-QIAGEN), with Nikon A1Si Laser-Scanning Confocal Microscope (Nikon, Tokyo, Japan) used for image analysis.

Western blotting and co-immunoprecipitation

The proteins extracted from human NP cells using Micro BCA Protein Assay Kit (Cat. No: 23235, Thermo Fisher Scientific) were separated into equal amounts using 10% SDS/PAGE (sodium dodecyl sulfate-polyacrylamide gels), and then electroblotted onto a polyvinylidene fluoride membranes (Bio-Rad Laboratories). The membranes were then incubated with primary antibodies as follows: anti-Col II, anti-Aggrecan, anti-ADAMTS4, anti-MMP9, anti-Caspase-3, anti-Bax, anti-P16, anti-p-ERK1/2, anti-ERK1/2, anti-GRB2, anti-SIRT6, and anti-GAPDH (ab34712, ab36861, ab185722, ab38898, ab13847, ab132503, ab151303, ab214362, ab184699, ab32111, ab191385, and ab9485; Abcam, Cambridge, UK). After washing, the membranes were then treated with 1/2000 secondary goat anti-rabbit antibody (Abcam, Cambridge, UK). The resulting patterns were then interpreted using the Quantity One version 4.50 software (Bio-Rad, Hercules, CA, USA). The Co-immunoprecipitation analysis was performed on basis of nuclear and cytoplasmic proteins. Extraction Kit (Thermo Scientific, 78833) was then used to extract nuclear and cytoplasmic proteins from the human NP cells, and the expression levels of GRB2 and SIRT6 detected using anti-GRB2 (ab32111, Abcam) and anti-SIRT6 (ab191385, Abcam) antibodies.

Immunofluorescence and TUNEL staining

Intervertebral discs were fixed, decalcified and embedded in 10% formalin, 10% EDTA, and paraffin, respectively. Sagittal sections of disc tissue were then cut at every 3 μm from the midsagittal plane. The sections were then stained with alcian blue for histological analysis. Masuda's method was then used for the grading score of the histological staining.[25] The cultured NP cells were then fixed, permeabilized and blocked with 4% paraformaldehyde, 0.3% Triton X-100, and 1% BSA, respectively. For the immunofluorescence analysis, the following primary antibodies were incubated with sections of cells: anti-Mmp9, anti-Col II antibody (ab73734, ab34712; Abcam, Cambridge, UK) at 4 °C overnight. The sections and cells were then treated with a secondary antibody for 20 min at room temperature, followed by the capturing of immunofluorescence images using a Zeiss LSM780 confocal microscope (CarlZeiss, Oberkochen, Germany). For the detection of apoptotic activity, TUNEL assay was conducted using a DeadEnd Colorimetric TUNEL System in accordance with the manual protocol (Cat. No: G7360, Promega).

Statistical analysis

All statistical analysis was performed using SPSS version 17.0 Software (SPSS Inc., Chicago, IL). The comparisons between two or more groups were analyzed using two-tailed unpaired Student's test or one-way ANOVA with Turkey's post hoc test. A p-value was considered statistically significant when less than 0.05.

Abbreviations

IDD: Intervertebral disc degeneration; NP: Nucleus pulposus; AF: Annulus fibrosus; miRNAs: MicroRNAs; SIRT6: Sirtuin 6; MAPK: Mitogen-activated protein kinase; ERK: Extracellular regulated protein kinases; FISH: Fluorescence in situ hybridization.

Declarations

Ethics approval and consent to participate

This study was approved by the Ethics Committee of The First Affiliated Hospital of Guangxi Medical University (2018-KY-NSFC-025) and in accordance with the declaration of Helsinki and carried out with informed consent from all patients.

Consent for publication

The patients' consent for publication was achieved in written form.

Availability of data and materials

The datasets used and/or analyzed during the current study are available from the corresponding author on reasonable request.

Competing interests

The authors declare no conflicts of interest.

Funding

This work was supported by the National Natural Science Foundation of China (81860406), Guangxi Natural Science Foundation (2018GXNSFAA281127), and Medical Excellence Award Funded by the Creative Research Development Grant from the First Affiliated Hospital of Guangxi Medical University.

Authors' contributions

Study design: H.J. and Q.W.; Data collection: J.W. and D.M.; Contribution of analytical tools: Z.X. and D.C.; Data analysis: H.J.; Manuscript preparation: H.J. and A.M.; All authors reviewed and approved the manuscript.

References

1. Luoma K, Riihimaki H, Luukkonen R, Raininko R, Viikari-Juntura E, Lamminen A. Low back pain in relation to lumbar disc degeneration. Spine (Phila Pa 1976). 2000;25:487–92.
2. Andersson GB. Epidemiological features of chronic low-back pain. Lancet. 1999;354:581–5.
3. Maniadakis N, Gray A. The economic burden of back pain in the UK. Pain. 2000;84:95–103.
4. Wang J, Tian Y, Phillips KL, Chiverton N, Haddock G, Bunning RA, Cross AK, Shapiro IM, Le Maitre CL, Risbud MV. Tumor necrosis factor alpha- and interleukin-1beta-dependent induction of CCL3 expression by nucleus pulposus cells promotes macrophage migration through CCR1. Arthritis Rheum. 2013;65:832–42.
5. Kepler CK, Ponnappan RK, Tannoury CA, Risbud MV, Anderson DG. The molecular basis of intervertebral disc degeneration. Spine J. 2013;13:318–30.
6. Kadow T, Sowa G, Vo N, Kang JD. Molecular basis of intervertebral disc degeneration and herniations: what are the important translational questions? Clin Orthop Relat Res. 2015;473:1903–12.
7. Radcliff KE, Kepler CK, Jakoi A, Sidhu GS, Rihn J, Vaccaro AR, Albert TJ, Hilibrand AS. Adjacent segment disease in the lumbar spine following different treatment interventions. Spine J. 2013;13:1339–49.
8. Moon SH, Nishida K, Gilbertson LG, Lee HM, Kim H, Hall RA, Robbins PD, Kang JD. Biologic response of human intervertebral disc cells to gene therapy cocktail. Spine (Phila Pa 1976). 2008;33:1850–5.
9. Seki S, Asanuma-Abe Y, Masuda K, Kawaguchi Y, Asanuma K, Muehleman C, Iwai A, Kimura T. Effect of small interference RNA (siRNA) for ADAMTS5 on intervertebral disc degeneration in the rabbit anular needle-puncture model. Arthritis Res Ther. 2009;11:R166.
10. Yamada K, Sudo H, Iwasaki K, Sasaki N, Higashi H, Kameda Y, Ito M, Takahata M, Abumi K, Minami A, Iwasaki N. Caspase 3 silencing inhibits biomechanical overload-induced intervertebral disk degeneration. Am J Pathol. 2014;184:753–64.
11. Liu Y, Yu T, Ma XX, Xiang HF, Hu YG, Chen BH. Lentivirus-mediated TGF-beta3, CTGF and TIMP1 gene transduction as a gene therapy for intervertebral disc degeneration in an in vivo rabbit model. Exp Ther Med. 2016;11:1399–404.
12. Wang SZ, Rui YF, Lu J, Wang C. Cell and molecular biology of intervertebral disc degeneration: current understanding and implications for potential therapeutic strategies. Cell Prolif. 2014;47:381–90.
13. Ameres SL, Zamore PD. Diversifying microRNA sequence and function. Nat Rev Mol Cell Biol. 2013;14:475–88.
14. Bartel DP. MicroRNAs: target recognition and regulatory functions. Cell. 2009;136:215–33.
15. Sun W, Julie Li YS, Huang HD, Shyy JY, Chien S. microRNA: a master regulator of cellular processes for bioengineering systems. Annu Rev Biomed Eng. 2010;12:1–27.

16. Nam JW, Rissland OS, Koppstein D, Abreu-Goodger C, Jan CH, Agarwal V, Yildirim MA, Rodriguez A, Bartel DP. Global analyses of the effect of different cellular contexts on microRNA targeting. Mol Cell. 2014;53:1031–43.
17. Miyaki S, Asahara H. Macro view of microRNA function in osteoarthritis. Nat Rev Rheumatol. 2012;8:543–52.
18. Ji ML, Lu J, Shi PL, Zhang XJ, Wang SZ, Chang Q, Chen H, Wang C. Dysregulated miR-98 Contributes to Extracellular Matrix Degradation by Targeting IL-6/STAT3 Signaling Pathway in Human Intervertebral Disc Degeneration. J Bone Miner Res. 2016;31:900–9.
19. Si HB, Zeng Y, Liu SY, Zhou ZK, Chen YN, Cheng JQ, Lu YR, Shen B. Intra-articular injection of microRNA-140 (miRNA-140) alleviates osteoarthritis (OA) progression by modulating extracellular matrix (ECM) homeostasis in rats. Osteoarthritis Cartilage. 2017;25:1698–707.
20. Nakamura A, Rampersaud YR, Nakamura S, Sharma A, Zeng F, Rossomacha E, Ali SA, Krawetz R, Haroon N, Perruccio AV, et al. microRNA-181a-5p antisense oligonucleotides attenuate osteoarthritis in facet and knee joints. Ann Rheum Dis. 2019;78:111–21.
21. Wang HQ, Yu XD, Liu ZH, Cheng X, Samartzis D, Jia LT, Wu SX, Huang J, Chen J, Luo ZJ. Deregulated miR-155 promotes Fas-mediated apoptosis in human intervertebral disc degeneration by targeting FADD and caspase-3. J Pathol. 2011;225:232–42.
22. Jing W, Jiang W. MicroRNA-93 regulates collagen loss by targeting MMP3 in human nucleus pulposus cells. Cell Prolif. 2015;48:284–92.
23. Ji ML, Jiang H, Zhang XJ, Shi PL, Li C, Wu H, Wu XT, Wang YT, Wang C, Lu J. Preclinical development of a microRNA-based therapy for intervertebral disc degeneration. Nat Commun. 2018;9:5051.
24. Dong W, Liu J, Lv Y, Wang F, Liu T, Sun S, Liao B, Shu Z. miR-640 aggravates intervertebral disc degeneration via NF-κB and WNT signalling pathway. Cell Prolif. 2019;52:e12664.
25. Masuda K, Aota Y, Muehleman C, Imai Y, Okuma M, Thonar EJ, Andersson GB, An HS. A novel rabbit model of mild, reproducible disc degeneration by an anulus needle puncture: correlation between the degree of disc injury and radiological and histological appearances of disc degeneration. Spine (Phila Pa 1976). 2005;30:5–14.
26. Han B, Zhu K, Li FC, Xiao YX, Feng J, Shi ZL, Lin M, Wang J, Chen QX. A simple disc degeneration model induced by percutaneous needle puncture in the rat tail. Spine (Phila Pa 1976). 2008;33:1925–34.
27. Tam V, Chan WCW, Leung VYL, Cheah KSE, Cheung KMC, Sakai D, McCann MR, Bedore J, Seguin CA, Chan D. Histological and reference system for the analysis of mouse intervertebral disc. J Orthop Res. 2018;36:233–43.
28. Haigis MC, Sinclair DA. Mammalian sirtuins: biological insights and disease relevance. Annu Rev Pathol. 2010;5:253–95.
29. Guarente L. Franklin H. Epstein Lecture: Sirtuins, aging, and medicine. N Engl J Med. 2011;364:2235–44.

30. Houtkooper RH, Pirinen E, Auwerx J. Sirtuins as regulators of metabolism and healthspan. Nat Rev Mol Cell Biol. 2012;13:225–38.
31. Zhang S, Jiang S, Wang H, Di W, Deng C, Jin Z, Yi W, Xiao X, Nie Y, Yang Y. SIRT6 protects against hepatic ischemia/reperfusion injury by inhibiting apoptosis and autophagy related cell death. Free Radic Biol Med. 2018;115:18–30.
32. Studer RK, Aboka AM, Gilbertson LG, Georgescu H, Sowa G, Vo N, Kang JD. p38 MAPK inhibition in nucleus pulposus cells: a potential target for treating intervertebral disc degeneration. Spine (Phila Pa 1976). 2007;32:2827–33.
33. Tian Y, Yuan W, Fujita N, Wang J, Wang H, Shapiro IM, Risbud MV. Inflammatory cytokines associated with degenerative disc disease control aggrecanase-1 (ADAMTS-4) expression in nucleus pulposus cells through MAPK and NF-kappaB. Am J Pathol. 2013;182:2310–21.
34. Liu C, Yang H, Gao F, Li X, An Y, Wang J, Jin A. Resistin Promotes Intervertebral Disc Degeneration by Upregulation of ADAMTS-5 Through p38 MAPK Signaling Pathway. Spine (Phila Pa 1976). 2016;41:1414–20.
35. Griffith JF, Wang YX, Antonio GE, Choi KC, Yu A, Ahuja AT, Leung PC. Modified Pfirrmann grading system for lumbar intervertebral disc degeneration. Spine (Phila Pa 1976). 2007;32:E708–12.
36. Yang F, Leung VY, Luk KD, Chan D, Cheung KM. Injury-induced sequential transformation of notochordal nucleus pulposus to chondrogenic and fibrocartilaginous phenotype in the mouse. J Pathol. 2009;218:113–21.

Figures

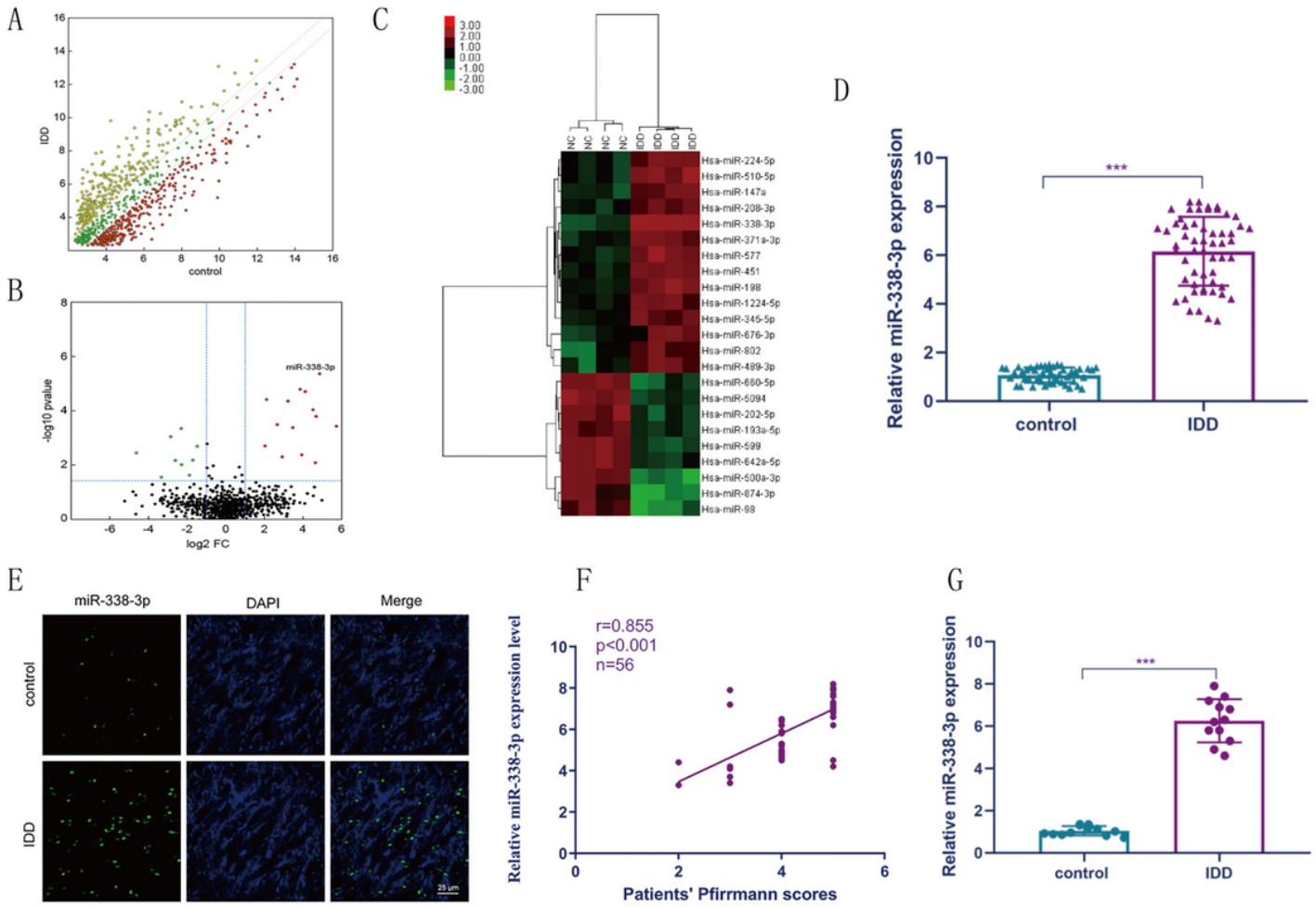

Figure 1

Differential expression of miRNAs between IDD patients and normal controls (A, B) Scatter plot and volcano plot showing the expression profiles of miRNA between IDD patients and normal controls. (C) Heat map illustrating 23 significantly dysregulated miRNAs in IDD patients (14 miRNAs upregulated and 9 miRNAs downregulated). (D) qRT-PCR showing the high degree of expression of miR-338-3p in IDD patients compared to that of the control group. (E) FISH analysis demonstrating the upregulation of miR-338-3p in NP tissues from patients with IDD. (Scale bar = 25 μm) (F) The significant positive correlation between miR-338-3p expression and Pfirmman grade of IDD (n=56, r = 0.855, P < 0.0001) (G) The upregulation of miR-338-3p in cultured NP cells of IDD patients but not in normal controls. ***P < 0.01

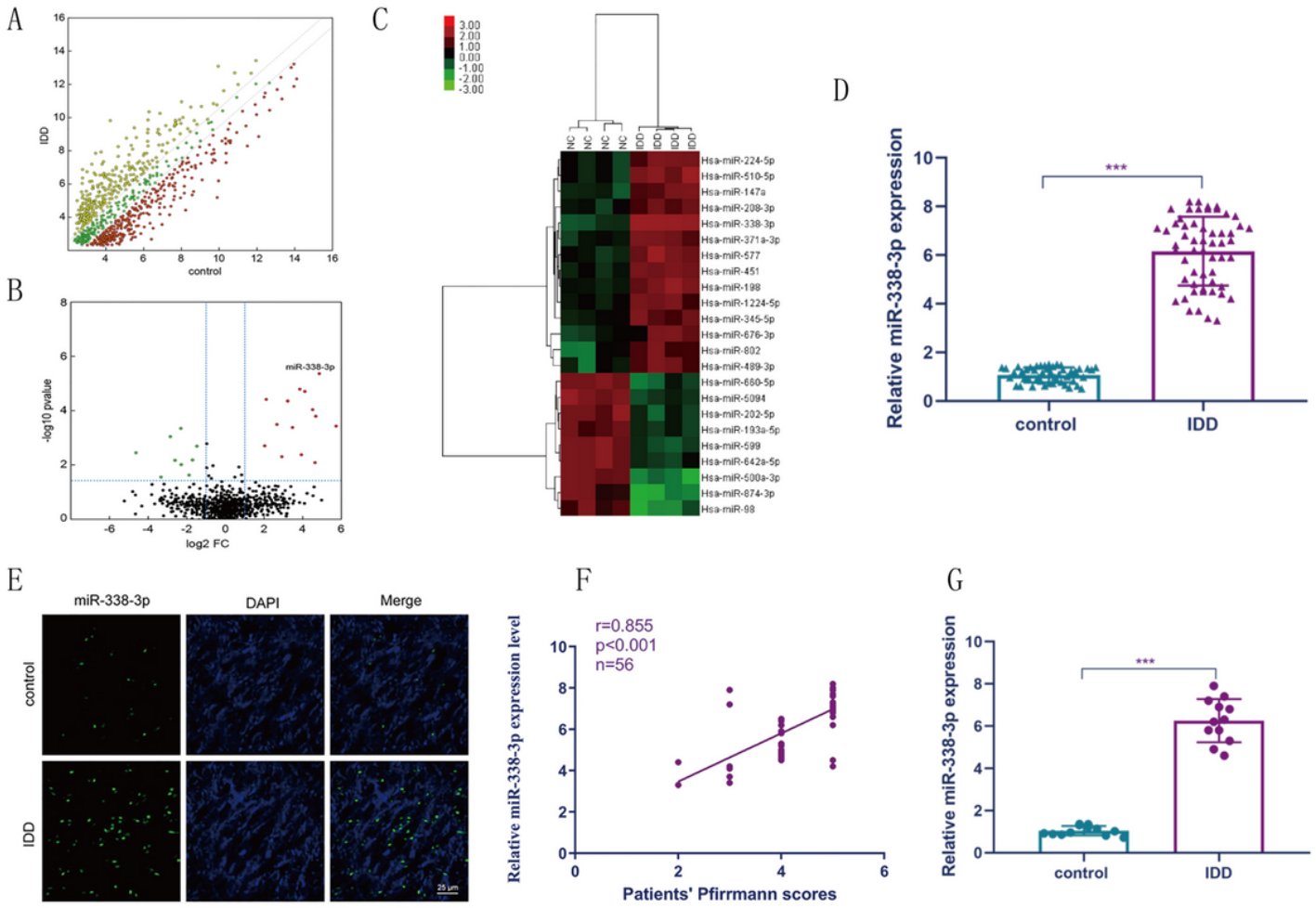

Figure 1

Differential expression of miRNAs between IDD patients and normal controls (A, B) Scatter plot and volcano plot showing the expression profiles of miRNA between IDD patients and normal controls. (C) Heat map illustrating 23 significantly dysregulated miRNAs in IDD patients (14 miRNAs upregulated and 9 miRNAs downregulated). (D) qRT-PCR showing the high degree of expression of miR-338-3p in IDD patients compared to that of the control group. (E) FISH analysis demonstrating the upregulation of miR-338-3p in NP tissues from patients with IDD. (Scale bar = 25 μm) (F) The significant positive correlation between miR-338-3p expression and Pfirmman grade of IDD (n=56, r = 0.855, P < 0.0001) (G) The upregulation of miR-338-3p in cultured NP cells of IDD patients but not in normal controls. ***P < 0.01

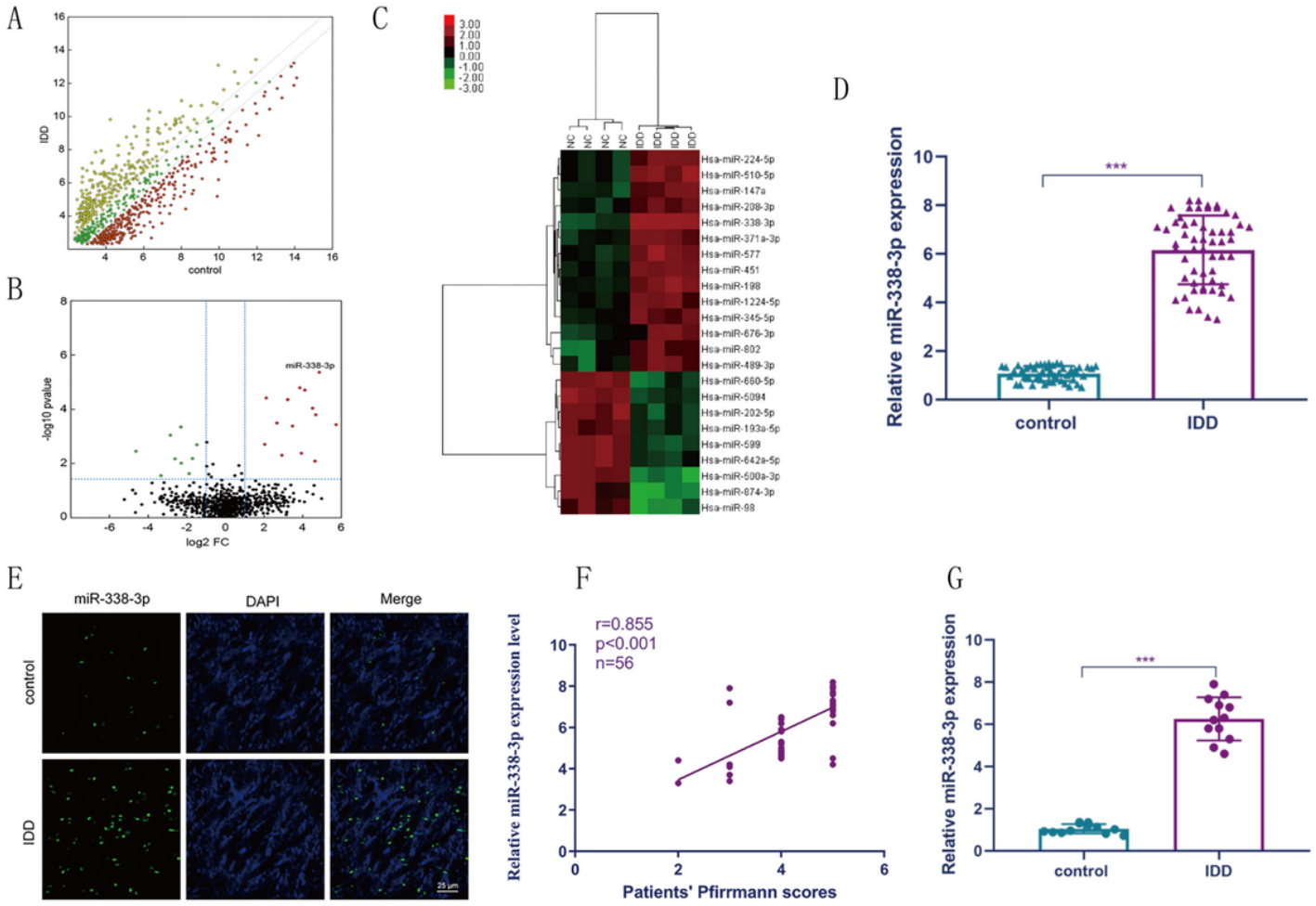

Figure 1

Differential expression of miRNAs between IDD patients and normal controls (A, B) Scatter plot and volcano plot showing the expression profiles of miRNA between IDD patients and normal controls. (C) Heat map illustrating 23 significantly dysregulated miRNAs in IDD patients (14 miRNAs upregulated and 9 miRNAs downregulated). (D) qRT-PCR showing the high degree of expression of miR-338-3p in IDD patients compared to that of the control group. (E) FISH analysis demonstrating the upregulation of miR-338-3p in NP tissues from patients with IDD. (Scale bar = 25 μm) (F) The significant positive correlation between miR-338-3p expression and Pfirmman grade of IDD (n=56, r = 0.855, P < 0.0001) (G) The upregulation of miR-338-3p in cultured NP cells of IDD patients but not in normal controls. ***P < 0.01

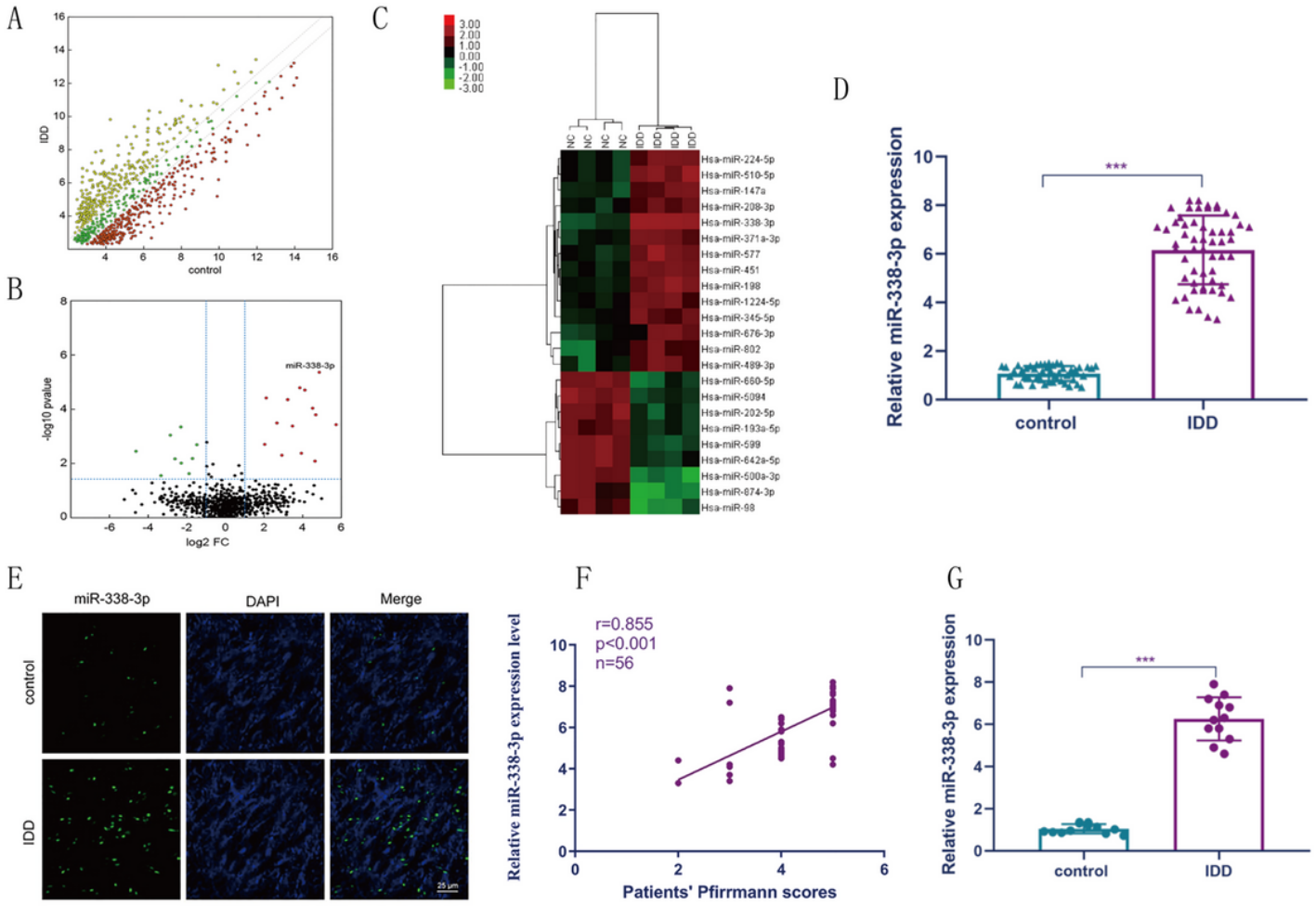

Figure 1

Differential expression of miRNAs between IDD patients and normal controls (A, B) Scatter plot and volcano plot showing the expression profiles of miRNA between IDD patients and normal controls. (C) Heat map illustrating 23 significantly dysregulated miRNAs in IDD patients (14 miRNAs upregulated and 9 miRNAs downregulated). (D) qRT-PCR showing the high degree of expression of miR-338-3p in IDD patients compared to that of the control group. (E) FISH analysis demonstrating the upregulation of miR-338-3p in NP tissues from patients with IDD. (Scale bar = 25 μm) (F) The significant positive correlation between miR-338-3p expression and Pfirmman grade of IDD (n=56, r = 0.855, P < 0.0001) (G) The upregulation of miR-338-3p in cultured NP cells of IDD patients but not in normal controls. ***P < 0.01

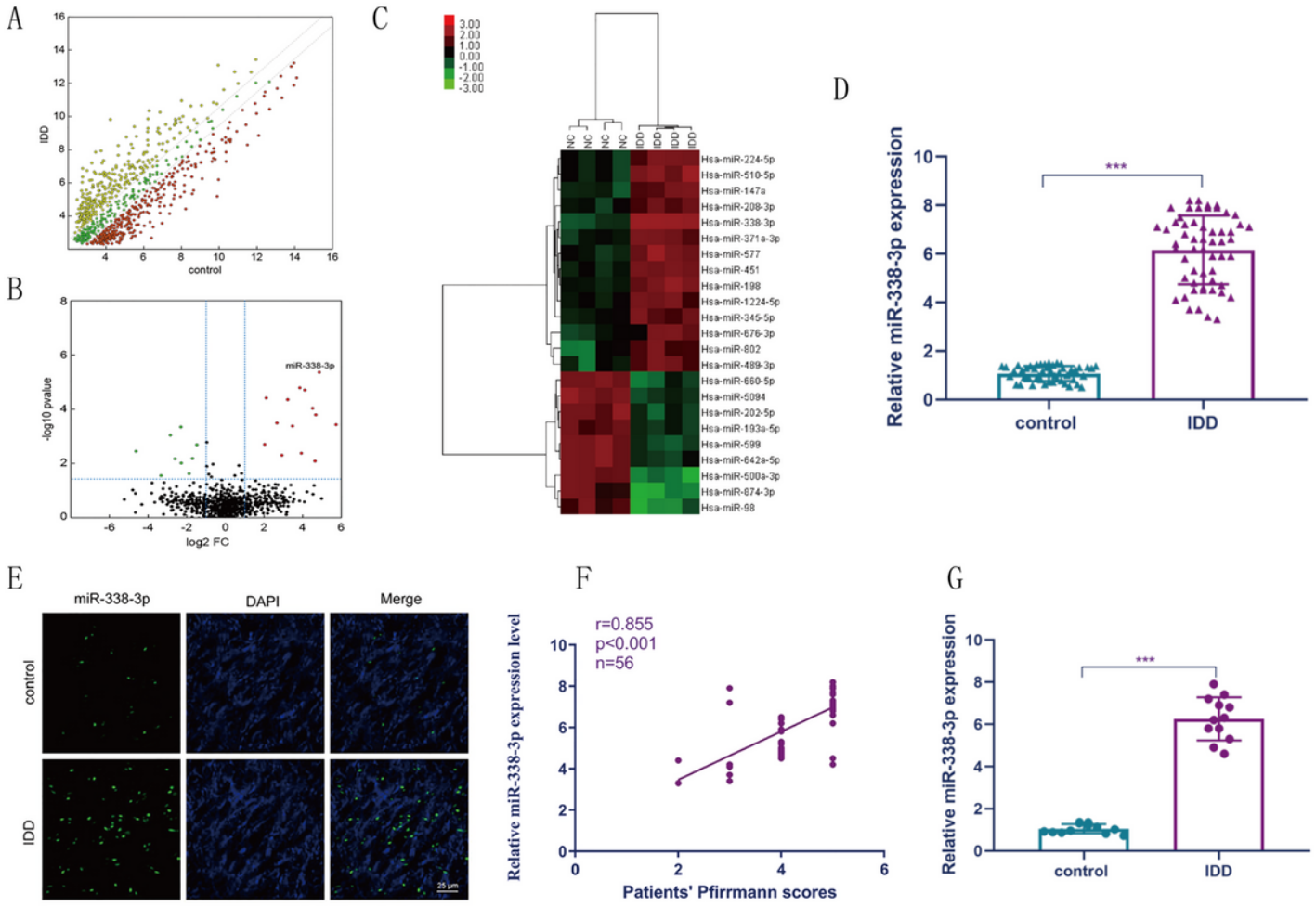

Figure 1

Differential expression of miRNAs between IDD patients and normal controls (A, B) Scatter plot and volcano plot showing the expression profiles of miRNA between IDD patients and normal controls. (C) Heat map illustrating 23 significantly dysregulated miRNAs in IDD patients (14 miRNAs upregulated and 9 miRNAs downregulated). (D) qRT-PCR showing the high degree of expression of miR-338-3p in IDD patients compared to that of the control group. (E) FISH analysis demonstrating the upregulation of miR-338-3p in NP tissues from patients with IDD. (Scale bar = 25 μm) (F) The significant positive correlation between miR-338-3p expression and Pfirmman grade of IDD (n=56, r = 0.855, P < 0.0001) (G) The upregulation of miR-338-3p in cultured NP cells of IDD patients but not in normal controls. ***P < 0.01

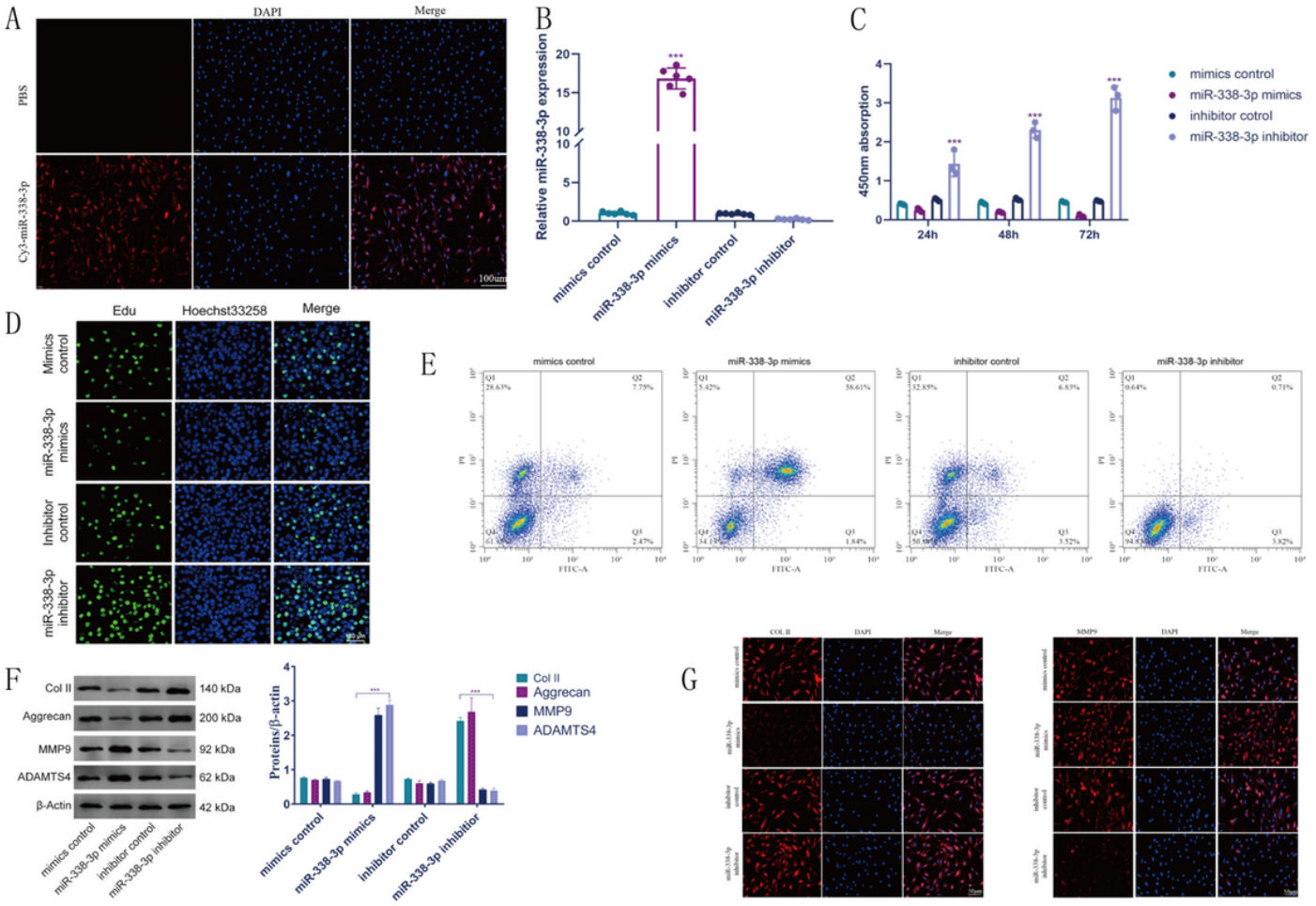

Figure 2

Functional analysis of miR-338-3p (A) Transfection of Cy3-oligonucleotides labeled miR-338-3p into cultured human NP cells. (Scale bar = 100 μm) (B) qRT-PCR showing transfection efficiency of miR-338-3p in human NP cells. (C, D) CCK8 and EdU assays showing the level of cellular proliferation in human NP cells transfected with miR-338-3p mimics or inhibitor. (Scale bar = 100 μm) (E) Flow cytometry showing apoptosis of human NP cells that were transfected into miR-338-3p mimics or inhibitor. (F) The expression levels of Col II, Aggrecan, MMP9 and ADAMTS4 detected using western blotting. (G) Immunofluorescence analysis of Col II and MMP9 expression levels. (Scale bar = 25 μm) ***P < 0.01

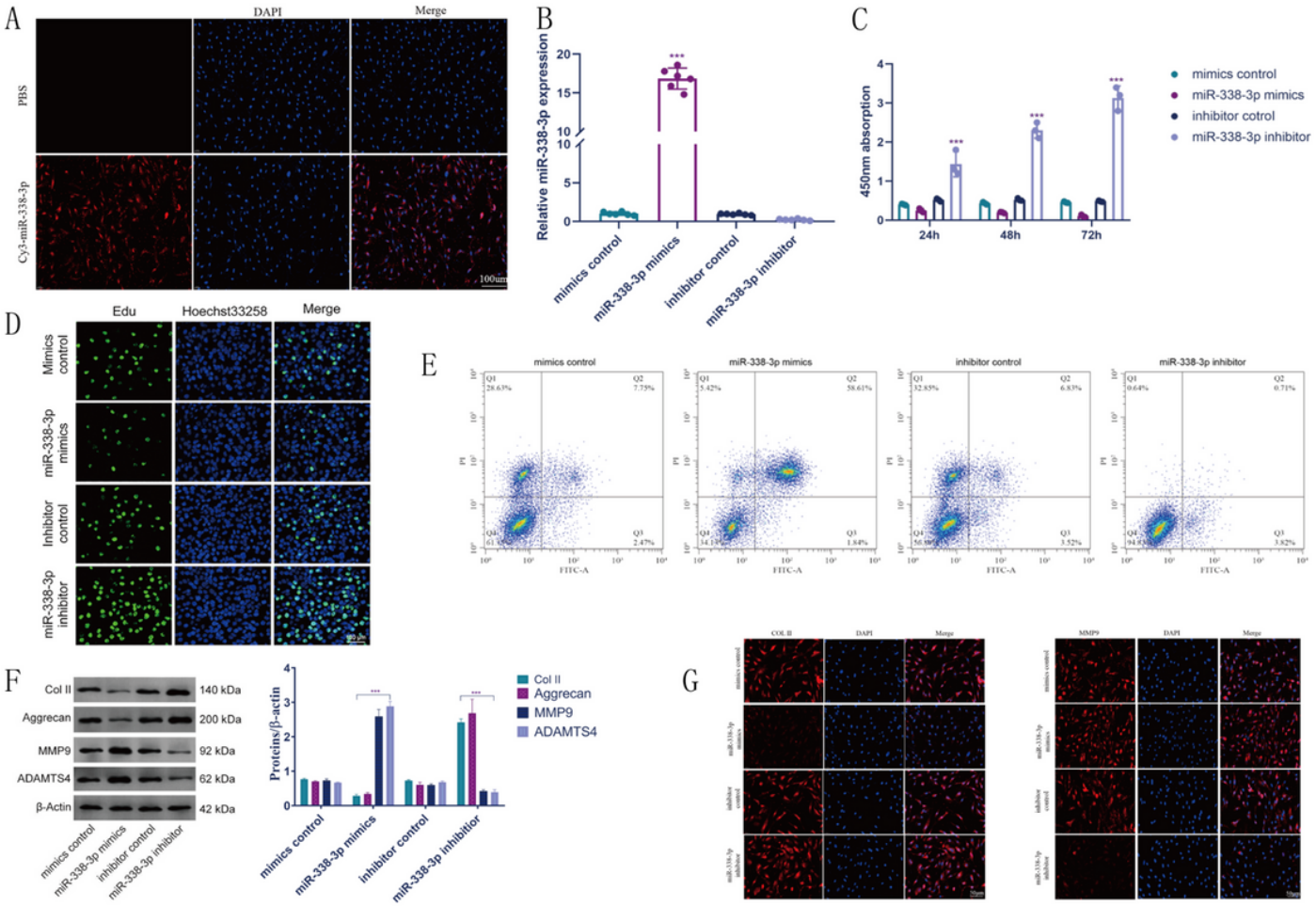

Figure 2

Functional analysis of miR-338-3p (A) Transfection of Cy3-oligonucleotides labeled miR-338-3p into cultured human NP cells. (Scale bar = 100 μm) (B) qRT-PCR showing transfection efficiency of miR-338-3p in human NP cells. (C, D) CCK8 and EdU assays showing the level of cellular proliferation in human NP cells transfected with miR-338-3p mimics or inhibitor. (Scale bar = 100 μm) (E) Flow cytometry showing apoptosis of human NP cells that were transfected into miR-338-3p mimics or inhibitor. (F) The expression levels of Col II, Aggrecan, MMP9 and ADAMTS4 detected using western blotting. (G) Immunofluorescence analysis of Col II and MMP9 expression levels. (Scale bar = 25 μm) ***P < 0.01

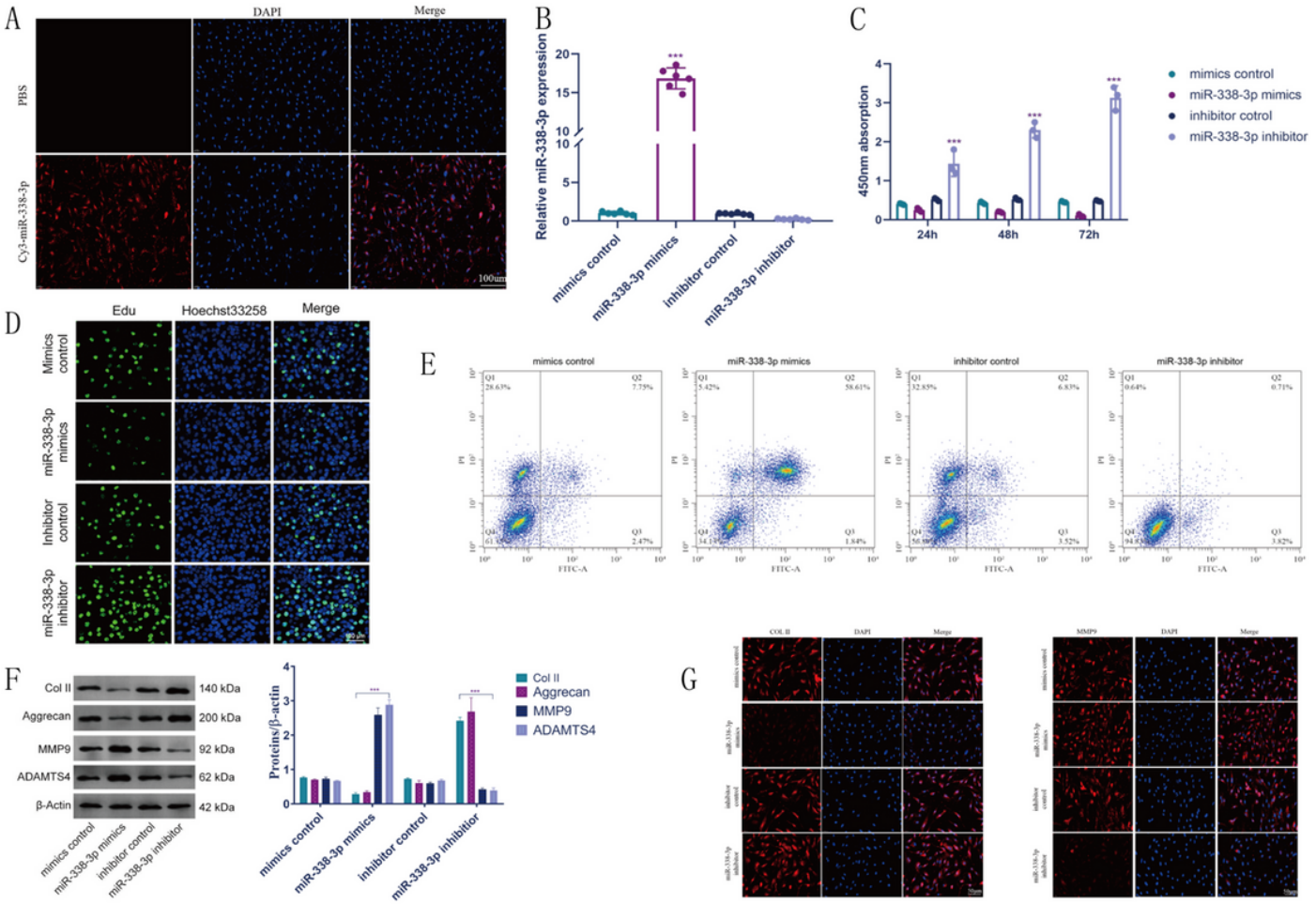

Figure 2

Functional analysis of miR-338-3p (A) Transfection of Cy3-oligonucleotides labeled miR-338-3p into cultured human NP cells. (Scale bar = 100 μm) (B) qRT-PCR showing transfection efficiency of miR-338-3p in human NP cells. (C, D) CCK8 and EdU assays showing the level of cellular proliferation in human NP cells transfected with miR-338-3p mimics or inhibitor. (Scale bar = 100 μm) (E) Flow cytometry showing apoptosis of human NP cells that were transfected into miR-338-3p mimics or inhibitor. (F) The expression levels of Col II, Aggrecan, MMP9 and ADAMTS4 detected using western blotting. (G) Immunofluorescence analysis of Col II and MMP9 expression levels. (Scale bar = 25 μm) ***P < 0.01

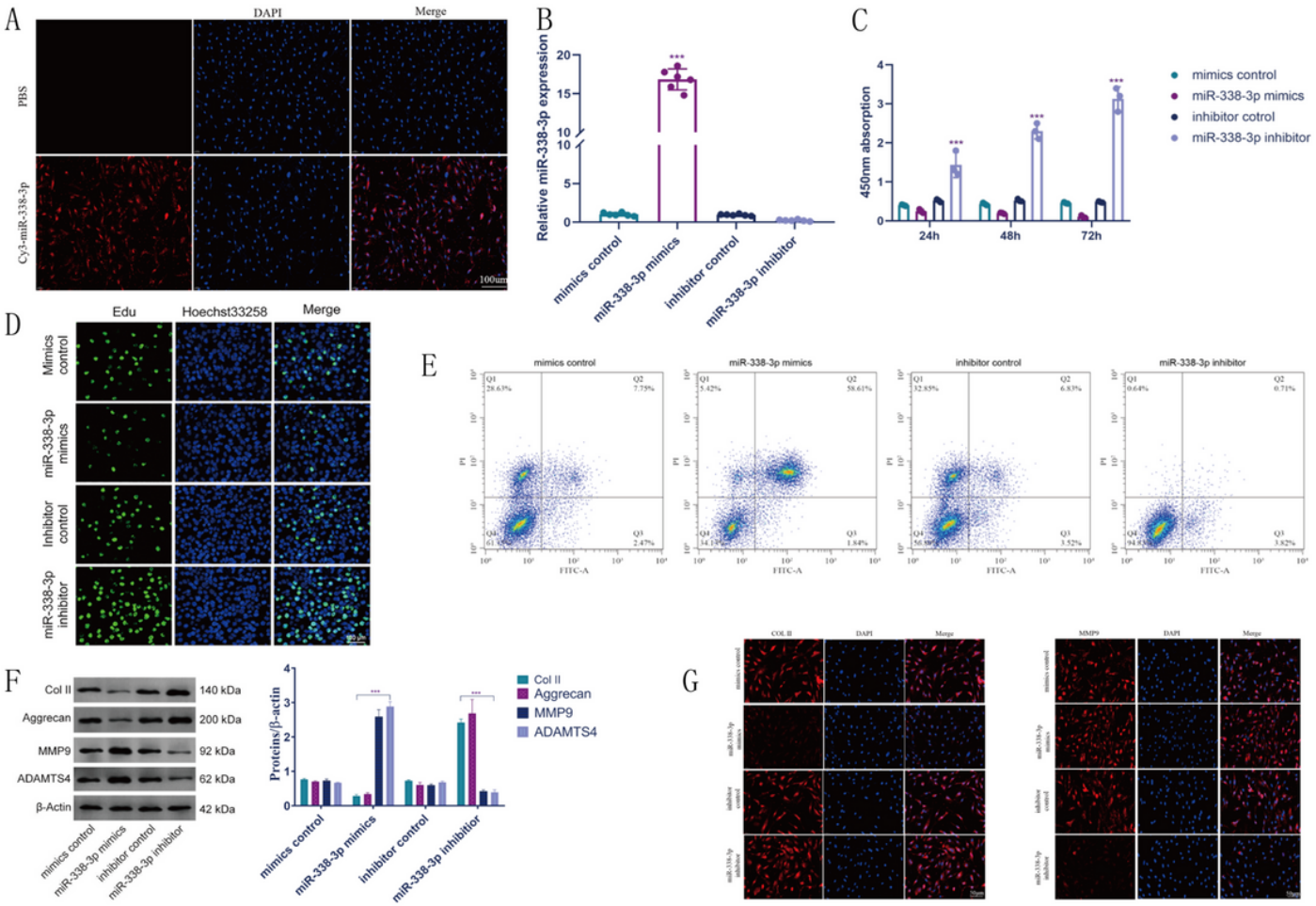

Figure 2

Functional analysis of miR-338-3p (A) Transfection of Cy3-oligonucleotides labeled miR-338-3p into cultured human NP cells. (Scale bar = 100 μm) (B) qRT-PCR showing transfection efficiency of miR-338-3p in human NP cells. (C, D) CCK8 and EdU assays showing the level of cellular proliferation in human NP cells transfected with miR-338-3p mimics or inhibitor. (Scale bar = 100 μm) (E) Flow cytometry showing apoptosis of human NP cells that were transfected into miR-338-3p mimics or inhibitor. (F) The expression levels of Col II, Aggrecan, MMP9 and ADAMTS4 detected using western blotting. (G) Immunofluorescence analysis of Col II and MMP9 expression levels. (Scale bar = 25 μm) ***P < 0.01

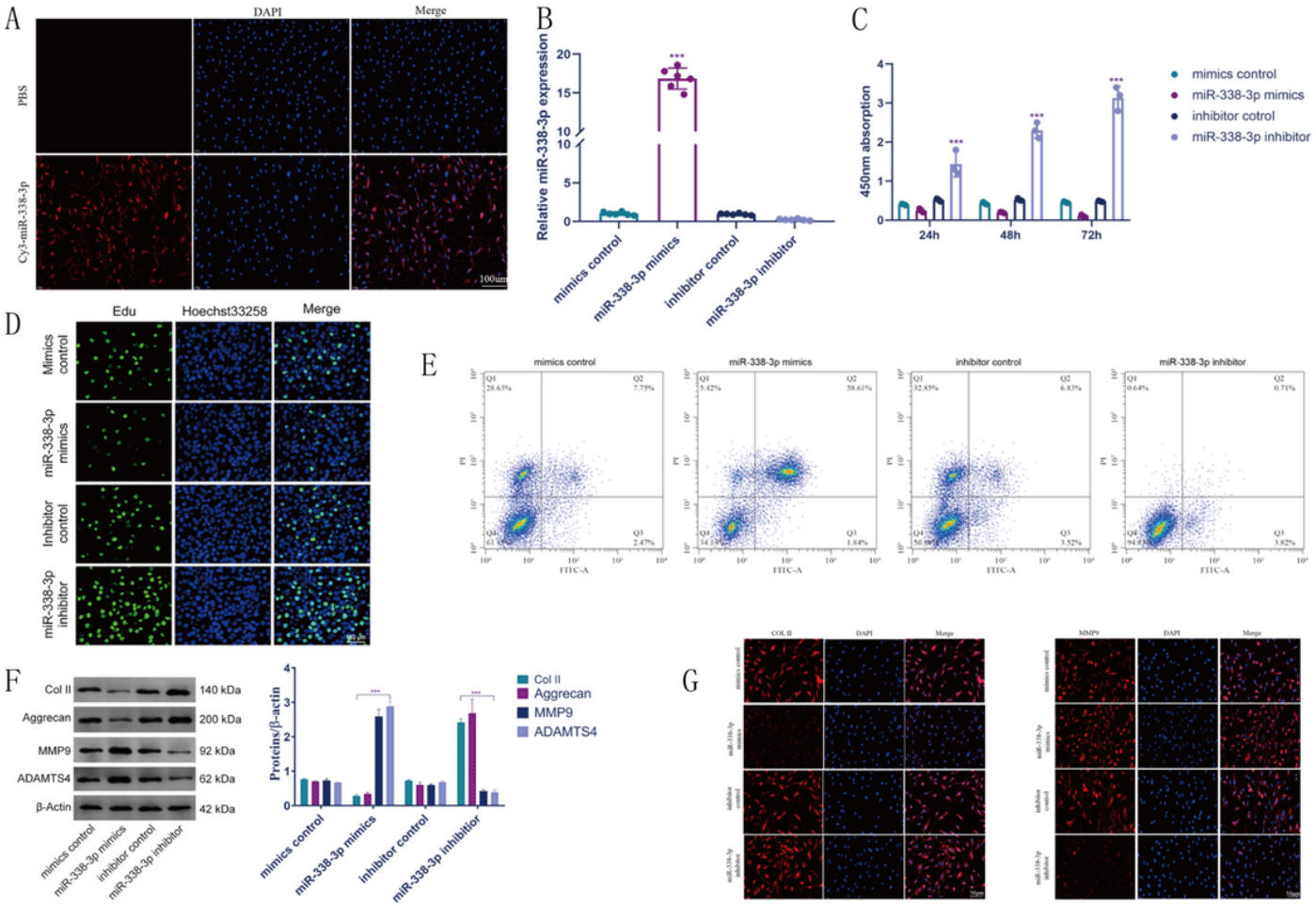

Figure 2

Functional analysis of miR-338-3p (A) Transfection of Cy3-oligonucleotides labeled miR-338-3p into cultured human NP cells. (Scale bar = 100 μm) (B) qRT-PCR showing transfection efficiency of miR-338-3p in human NP cells. (C, D) CCK8 and EdU assays showing the level of cellular proliferation in human NP cells transfected with miR-338-3p mimics or inhibitor. (Scale bar = 100 μm) (E) Flow cytometry showing apoptosis of human NP cells that were transfected into miR-338-3p mimics or inhibitor. (F) The expression levels of Col II, Aggrecan, MMP9 and ADAMTS4 detected using western blotting. (G) Immunofluorescence analysis of Col II and MMP9 expression levels. (Scale bar = 25 μm) ***P < 0.01

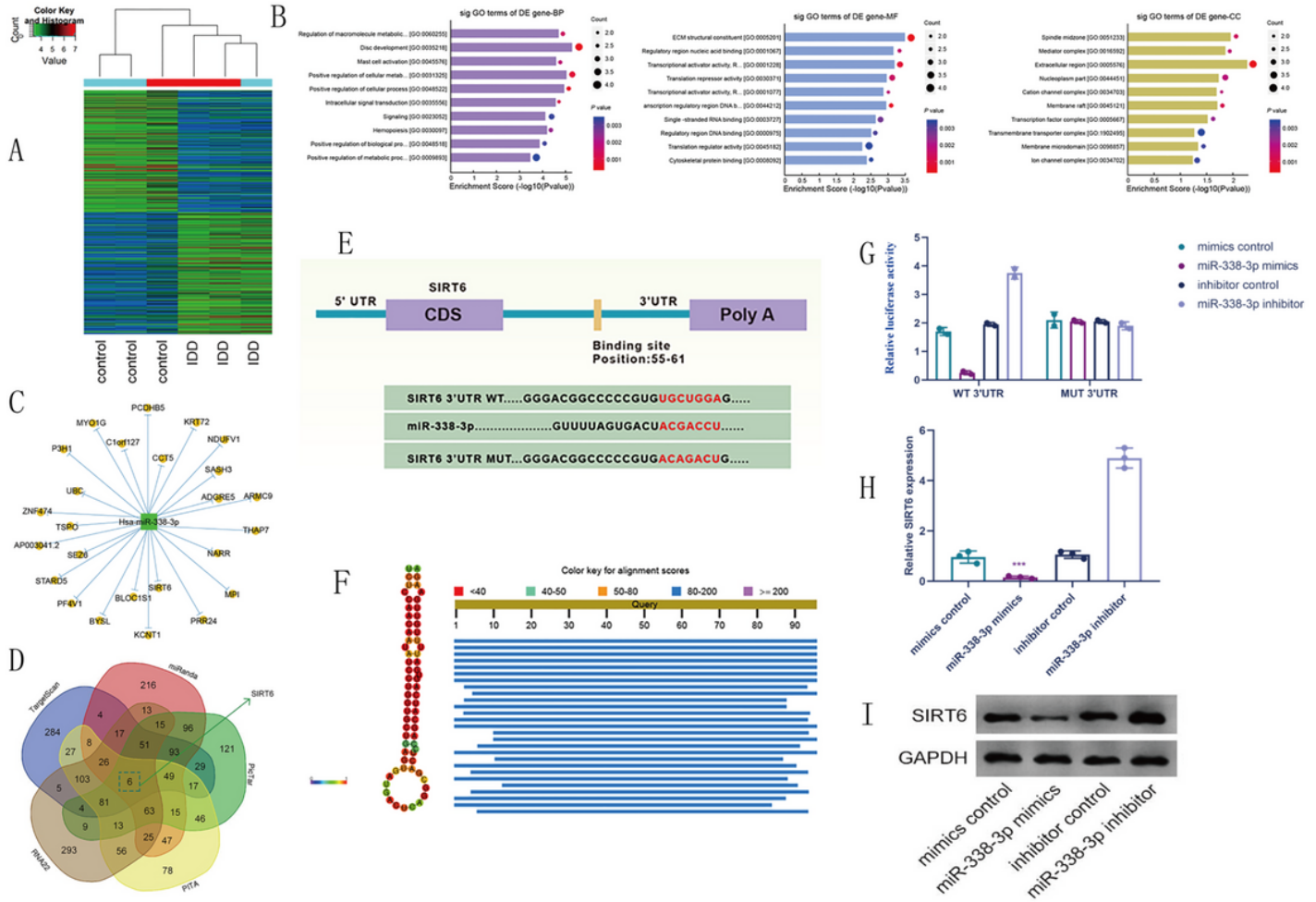

Figure 3

SIRT6 as a direct target gene of miR-338-3p (A) Microarray analysis showing the differential gene expressions between patients with IDD and normal controls. (B) Gene ontology analysis showing the top-ranked enrichment scores of downregulated GO terms. (C, D) Identification of SIRT6 as a potential regulatory target of miR-338-3p. (E) Sequential alignment showing the binding sites between miR-338-3p and SIRT6. (F) Computational alignment scores indicating high conservation of miR-338-3p. (G) The relative luciferase activity detection in human NP cells co-transfected with miR-338-3p mimic/inhibitor and SIRT6 3'UTR-wild/mutant-type reporter plasmids. (H, I) Analysis of the expression levels of SIRT6 mRNA and protein via qRT-PCR and western blotting following transfection with miR-338-3p mimics/inhibitor in human NP cells. ***P < 0.01

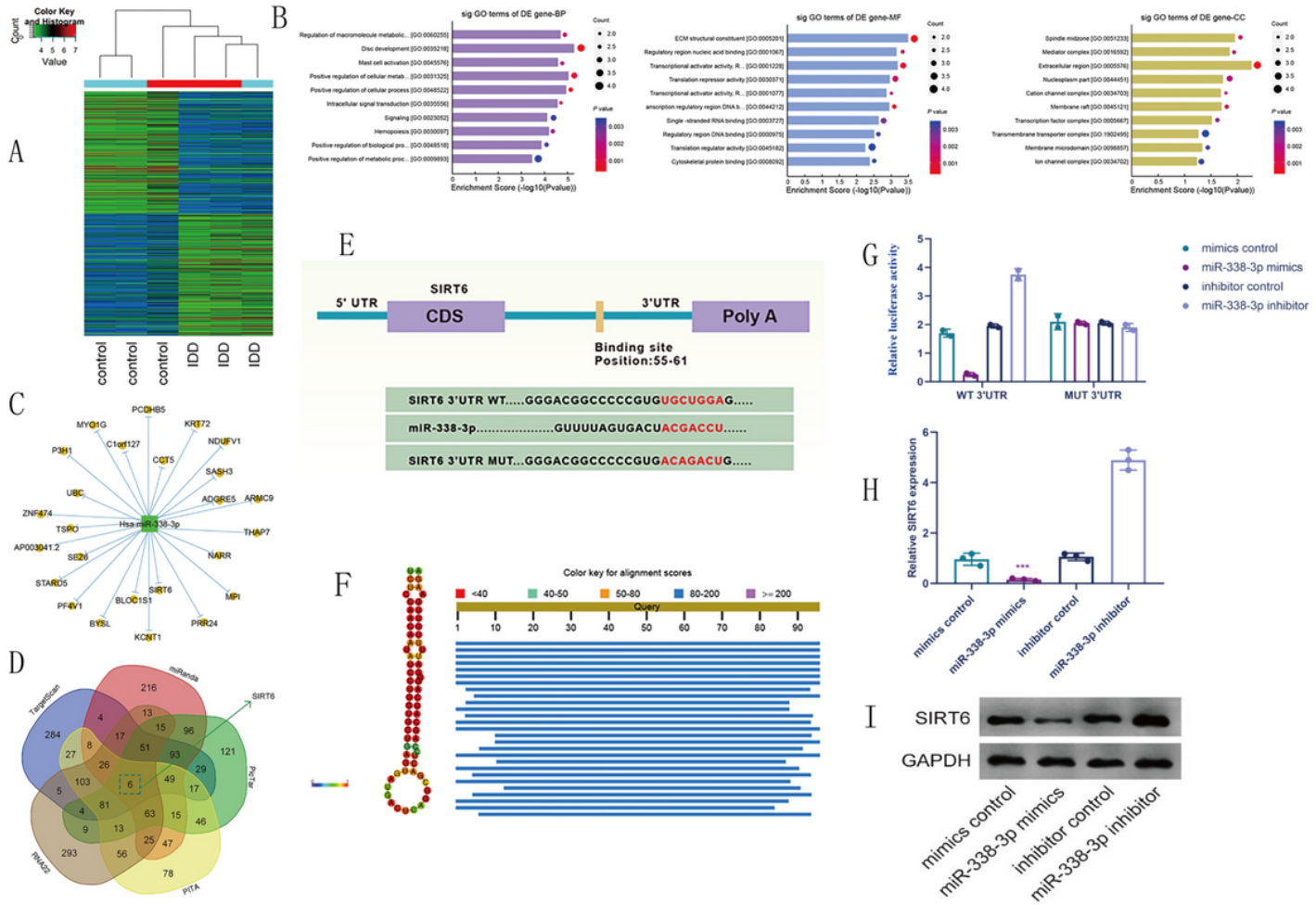

Figure 3

SIRT6 as a direct target gene of miR-338-3p (A) Microarray analysis showing the differential gene expressions between patients with IDD and normal controls. (B) Gene ontology analysis showing the top-ranked enrichment scores of downregulated GO terms. (C, D) Identification of SIRT6 as a potential regulatory target of miR-338-3p. (E) Sequential alignment showing the binding sites between miR-338-3p and SIRT6. (F) Computational alignment scores indicating high conservation of miR-338-3p. (G) The relative luciferase activity detection in human NP cells co-transfected with miR-338-3p mimic/inhibitor and SIRT6 3'UTR-wild/mutant-type reporter plasmids. (H, I) Analysis of the expression levels of SIRT6 mRNA and protein via qRT-PCR and western blotting following transfection with miR-338-3p mimics/inhibitor in human NP cells. ***P < 0.01

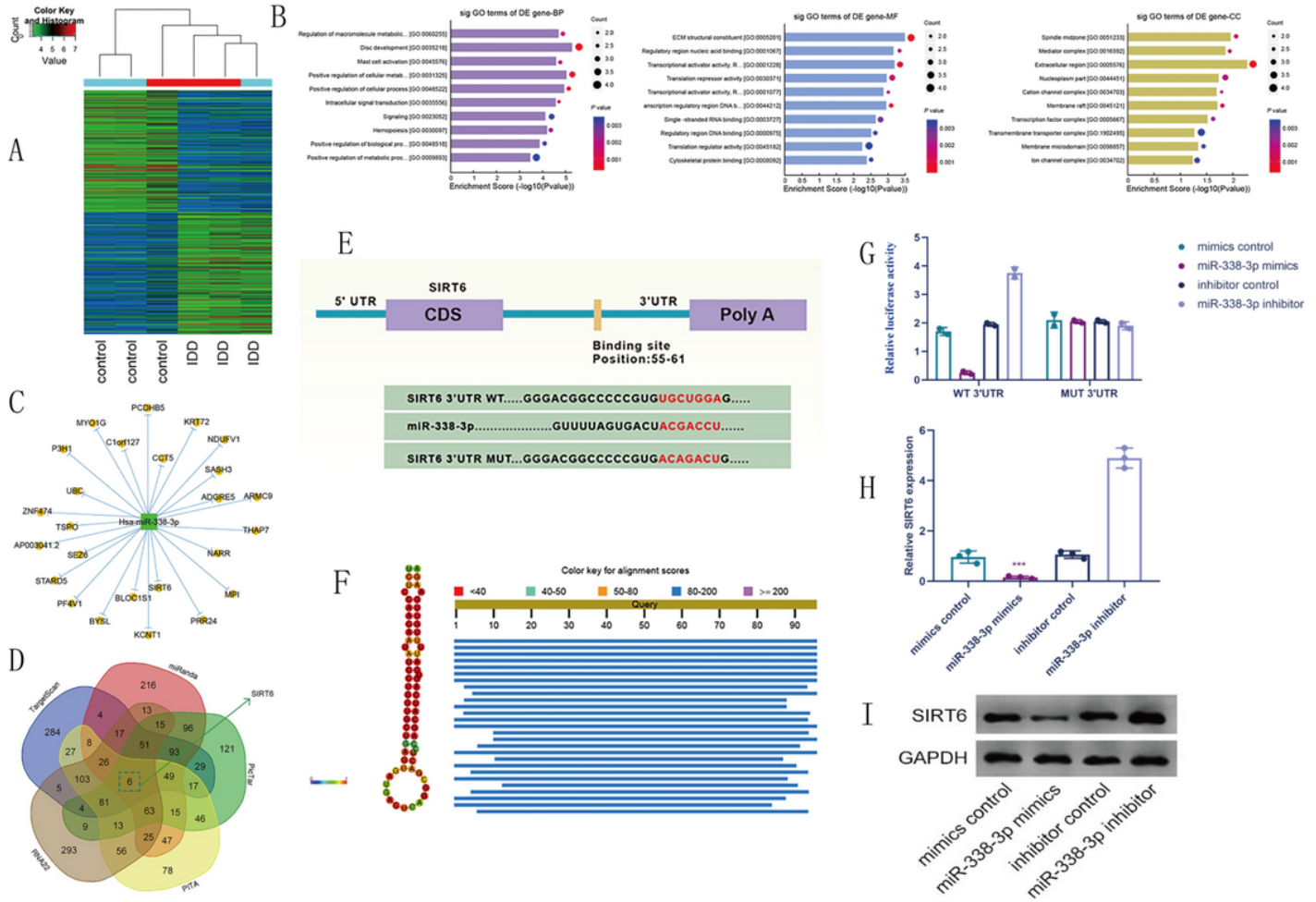

Figure 3

SIRT6 as a direct target gene of miR-338-3p (A) Microarray analysis showing the differential gene expressions between patients with IDD and normal controls. (B) Gene ontology analysis showing the top-ranked enrichment scores of downregulated GO terms. (C, D) Identification of SIRT6 as a potential regulatory target of miR-338-3p. (E) Sequential alignment showing the binding sites between miR-338-3p and SIRT6. (F) Computational alignment scores indicating high conservation of miR-338-3p. (G) The relative luciferase activity detection in human NP cells co-transfected with miR-338-3p mimic/inhibitor and SIRT6 3'UTR-wild/mutant-type reporter plasmids. (H, I) Analysis of the expression levels of SIRT6 mRNA and protein via qRT-PCR and western blotting following transfection with miR-338-3p mimics/inhibitor in human NP cells. ***P < 0.01

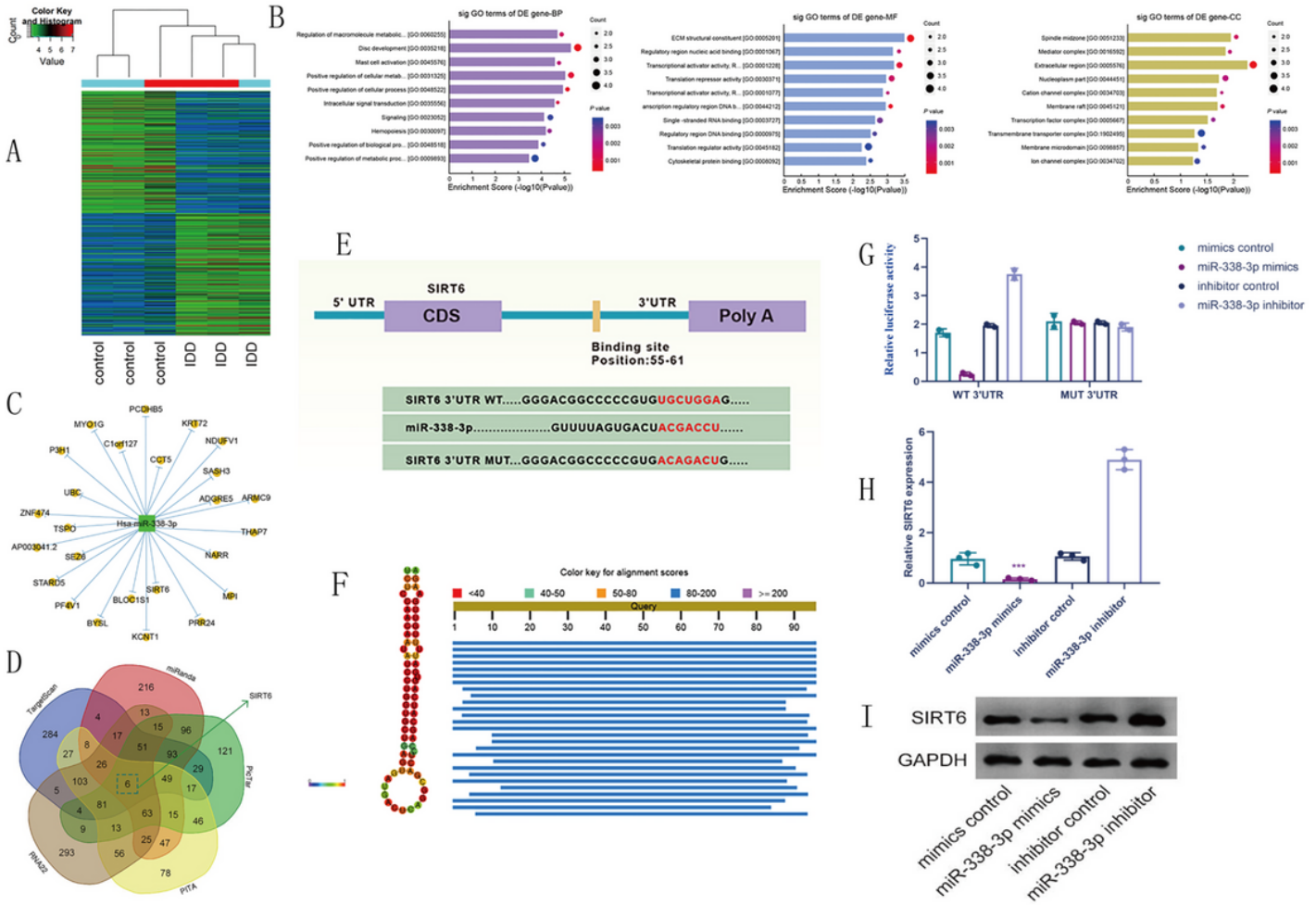

Figure 3

SIRT6 as a direct target gene of miR-338-3p (A) Microarray analysis showing the differential gene expressions between patients with IDD and normal controls. (B) Gene ontology analysis showing the top-ranked enrichment scores of downregulated GO terms. (C, D) Identification of SIRT6 as a potential regulatory target of miR-338-3p. (E) Sequential alignment showing the binding sites between miR-338-3p and SIRT6. (F) Computational alignment scores indicating high conservation of miR-338-3p. (G) The relative luciferase activity detection in human NP cells co-transfected with miR-338-3p mimic/inhibitor and SIRT6 3'UTR-wild/mutant-type reporter plasmids. (H, I) Analysis of the expression levels of SIRT6 mRNA and protein via qRT-PCR and western blotting following transfection with miR-338-3p mimics/inhibitor in human NP cells. ***P < 0.01

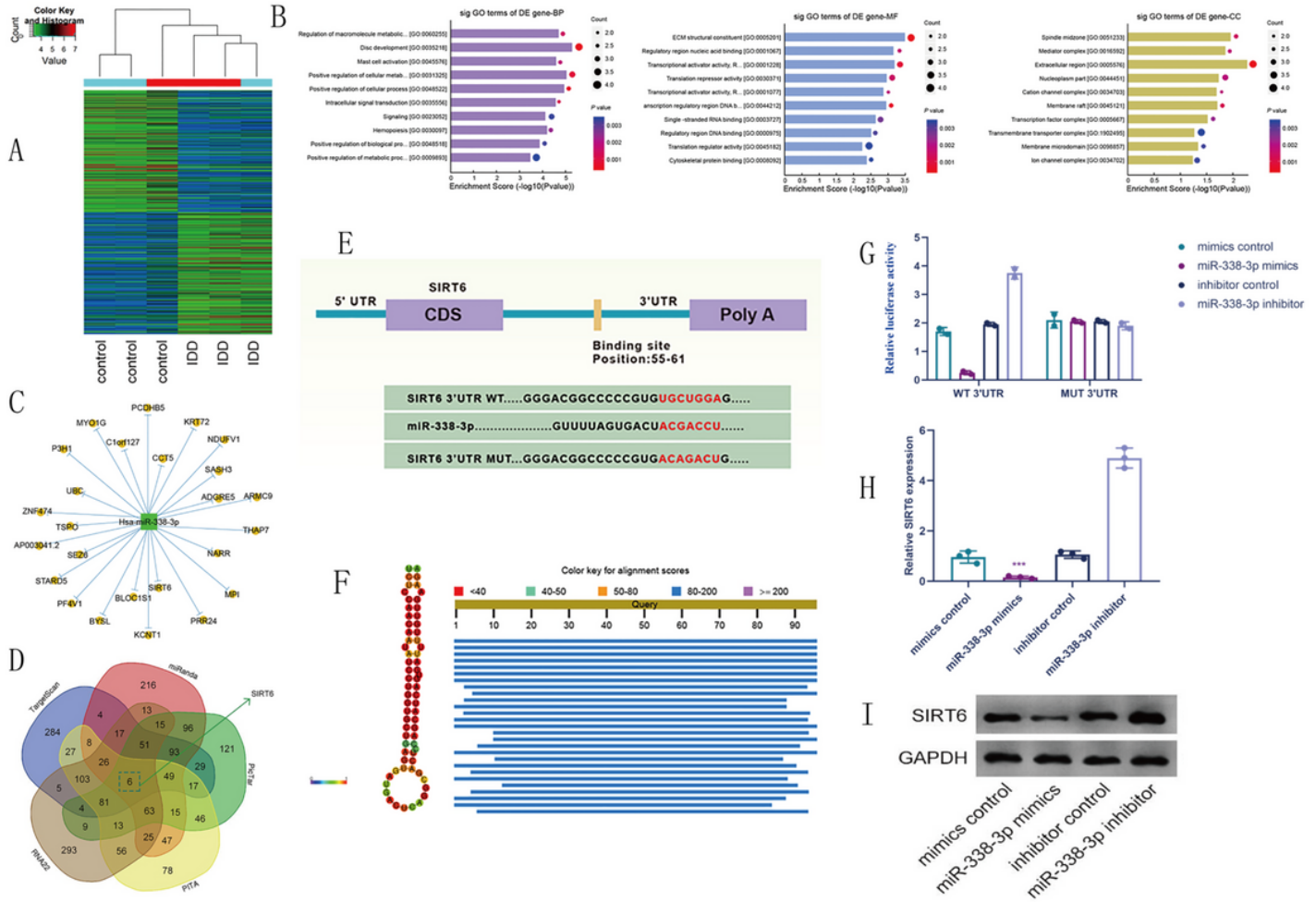

Figure 3

SIRT6 as a direct target gene of miR-338-3p (A) Microarray analysis showing the differential gene expressions between patients with IDD and normal controls. (B) Gene ontology analysis showing the top-ranked enrichment scores of downregulated GO terms. (C, D) Identification of SIRT6 as a potential regulatory target of miR-338-3p. (E) Sequential alignment showing the binding sites between miR-338-3p and SIRT6. (F) Computational alignment scores indicating high conservation of miR-338-3p. (G) The relative luciferase activity detection in human NP cells co-transfected with miR-338-3p mimic/inhibitor and SIRT6 3'UTR-wild/mutant-type reporter plasmids. (H, I) Analysis of the expression levels of SIRT6 mRNA and protein via qRT-PCR and western blotting following transfection with miR-338-3p mimics/inhibitor in human NP cells. ***P < 0.01

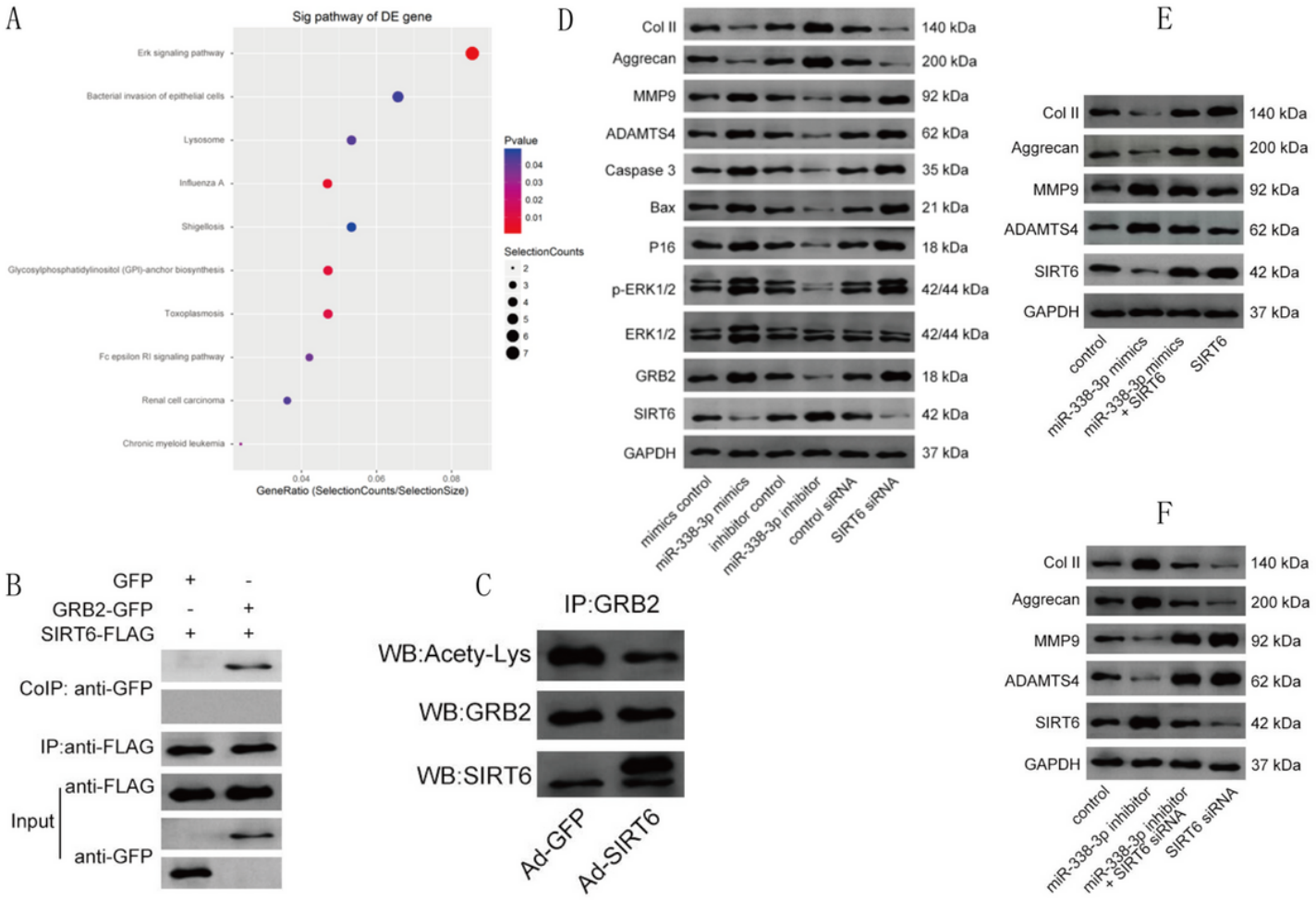

Figure 4

The modulation of miR-338-3p on SIRT6/MAPK/ERK signaling pathway. (A) KEGG analysis showing MAPK/ERK signaling pathway among the top-ranked pathways enriched with miRNAs downregulated in IDD samples. (B, C) Co-immunoprecipitation showing interactions between SIRT6 and GRB2. The deacetylated of GRB2 by SIRT6 resulting in its increased expression. (D)The expression levels of the proteins SIRT6, GRB2, ERK1/2, p-ERK1/2, P16, Bax, Caspase, Col II, Aggrecan, MMP9, and ADAMTS4 in human NP cells treated with miR-338-3p mimics/inhibitor and their negative controls siRNA, or SIRT6 siRNA. (E) The transfection of miR-338-3p mimics resulted in decreased expression levels of Col II and Aggrecan, whereas restoration of SIRT6 expression reversed this effect. Similarly, SIRT6 overexpression inhibited MMP9 and ADAMTS4 expressions, whereas miR-338-3p mimics reversed this decrease. (F) miR-338-3p inhibitor increased Col II and Aggrecan expressions, whereas silencing of SIRT6 stopped this effect. Similarly, SIRT6 knockdown increased MMP9 and ADAMTS4 expressions, whereas miR-338-3p inhibitor prevented this increase.

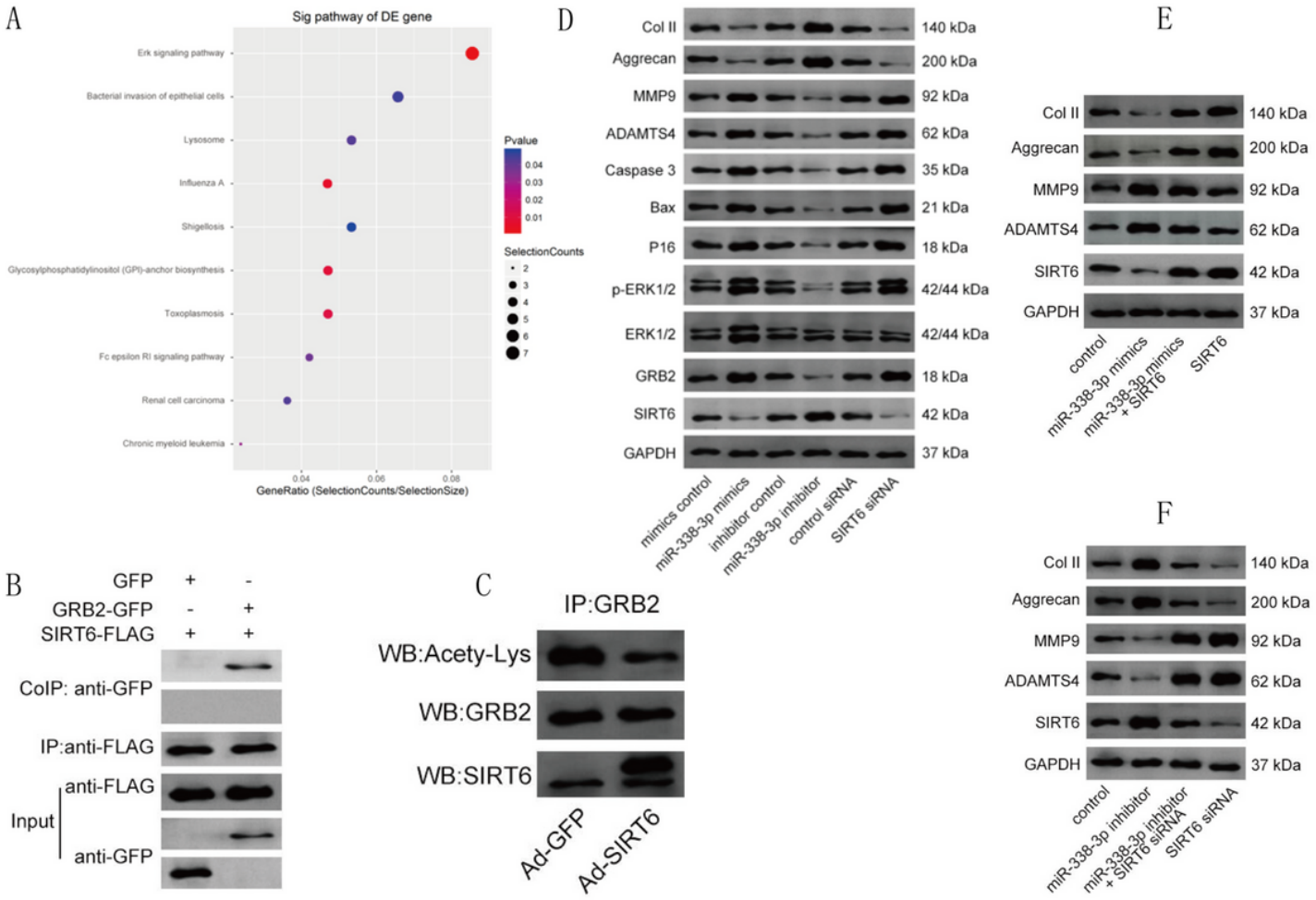

Figure 4

The modulation of miR-338-3p on SIRT6/MAPK/ERK signaling pathway. (A) KEGG analysis showing MAPK/ERK signaling pathway among the top-ranked pathways enriched with miRNAs downregulated in IDD samples. (B, C) Co-immunoprecipitation showing interactions between SIRT6 and GRB2. The deacetylated of GRB2 by SIRT6 resulting in its increased expression. (D)The expression levels of the proteins SIRT6, GRB2, ERK1/2, p-ERK1/2, P16, Bax, Caspase, Col II, Aggrecan, MMP9, and ADAMTS4 in human NP cells treated with miR-338-3p mimics/inhibitor and their negative controls siRNA, or SIRT6 siRNA. (E) The transfection of miR-338-3p mimics resulted in decreased expression levels of Col II and Aggrecan, whereas restoration of SIRT6 expression reversed this effect. Similarly, SIRT6 overexpression inhibited MMP9 and ADAMTS4 expressions, whereas miR-338-3p mimics reversed this decrease. (F) miR-338-3p inhibitor increased Col II and Aggrecan expressions, whereas silencing of SIRT6 stopped this effect. Similarly, SIRT6 knockdown increased MMP9 and ADAMTS4 expressions, whereas miR-338-3p inhibitor prevented this increase.

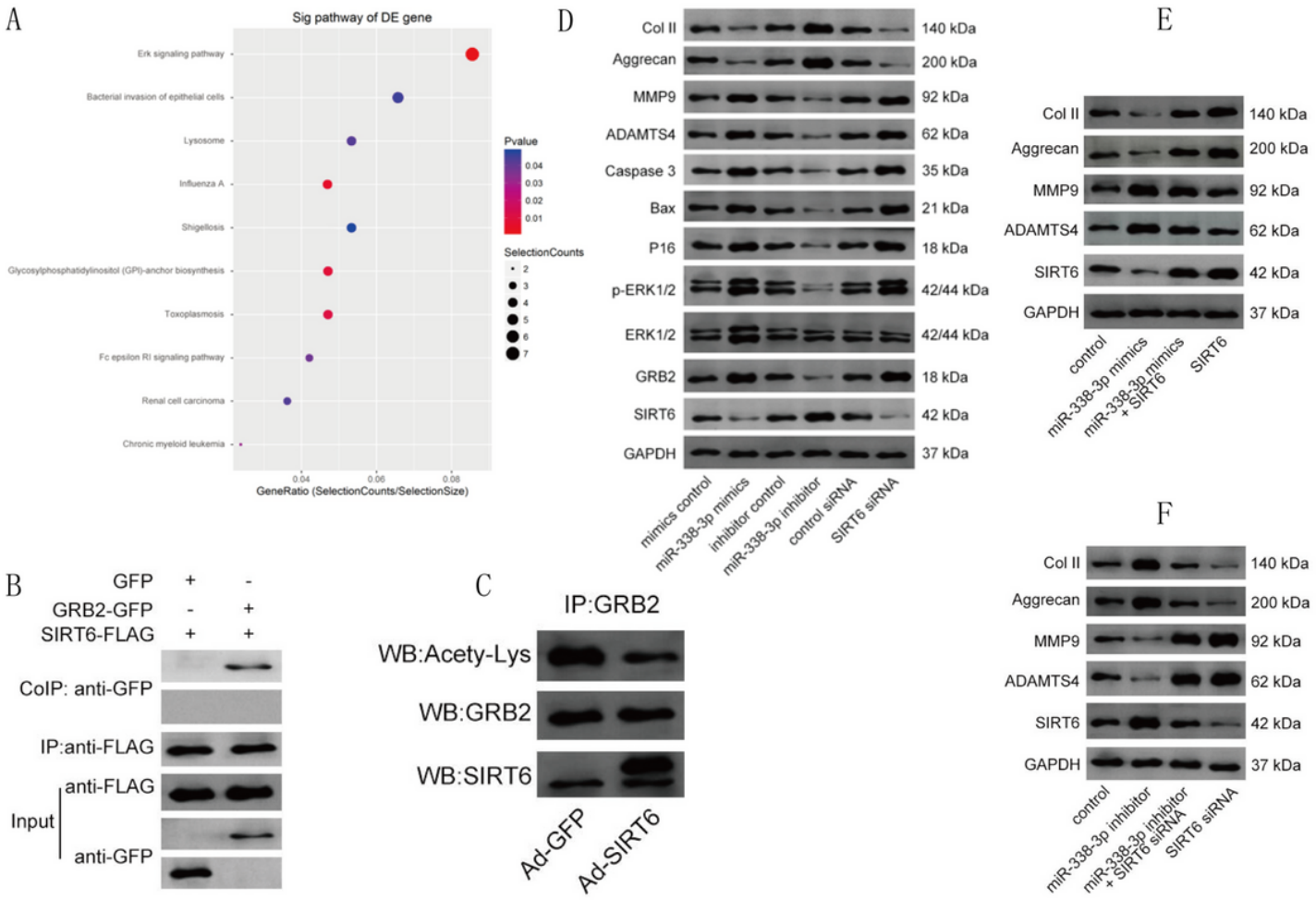

Figure 4

The modulation of miR-338-3p on SIRT6/MAPK/ERK signaling pathway. (A) KEGG analysis showing MAPK/ERK signaling pathway among the top-ranked pathways enriched with miRNAs downregulated in IDD samples. (B, C) Co-immunoprecipitation showing interactions between SIRT6 and GRB2. The deacetylated of GRB2 by SIRT6 resulting in its increased expression. (D)The expression levels of the proteins SIRT6, GRB2, ERK1/2, p-ERK1/2, P16, Bax, Caspase, Col II, Aggrecan, MMP9, and ADAMTS4 in human NP cells treated with miR-338-3p mimics/inhibitor and their negative controls siRNA, or SIRT6 siRNA. (E) The transfection of miR-338-3p mimics resulted in decreased expression levels of Col II and Aggrecan, whereas restoration of SIRT6 expression reversed this effect. Similarly, SIRT6 overexpression inhibited MMP9 and ADAMTS4 expressions, whereas miR-338-3p mimics reversed this decrease. (F) miR-338-3p inhibitor increased Col II and Aggrecan expressions, whereas silencing of SIRT6 stopped this effect. Similarly, SIRT6 knockdown increased MMP9 and ADAMTS4 expressions, whereas miR-338-3p inhibitor prevented this increase.

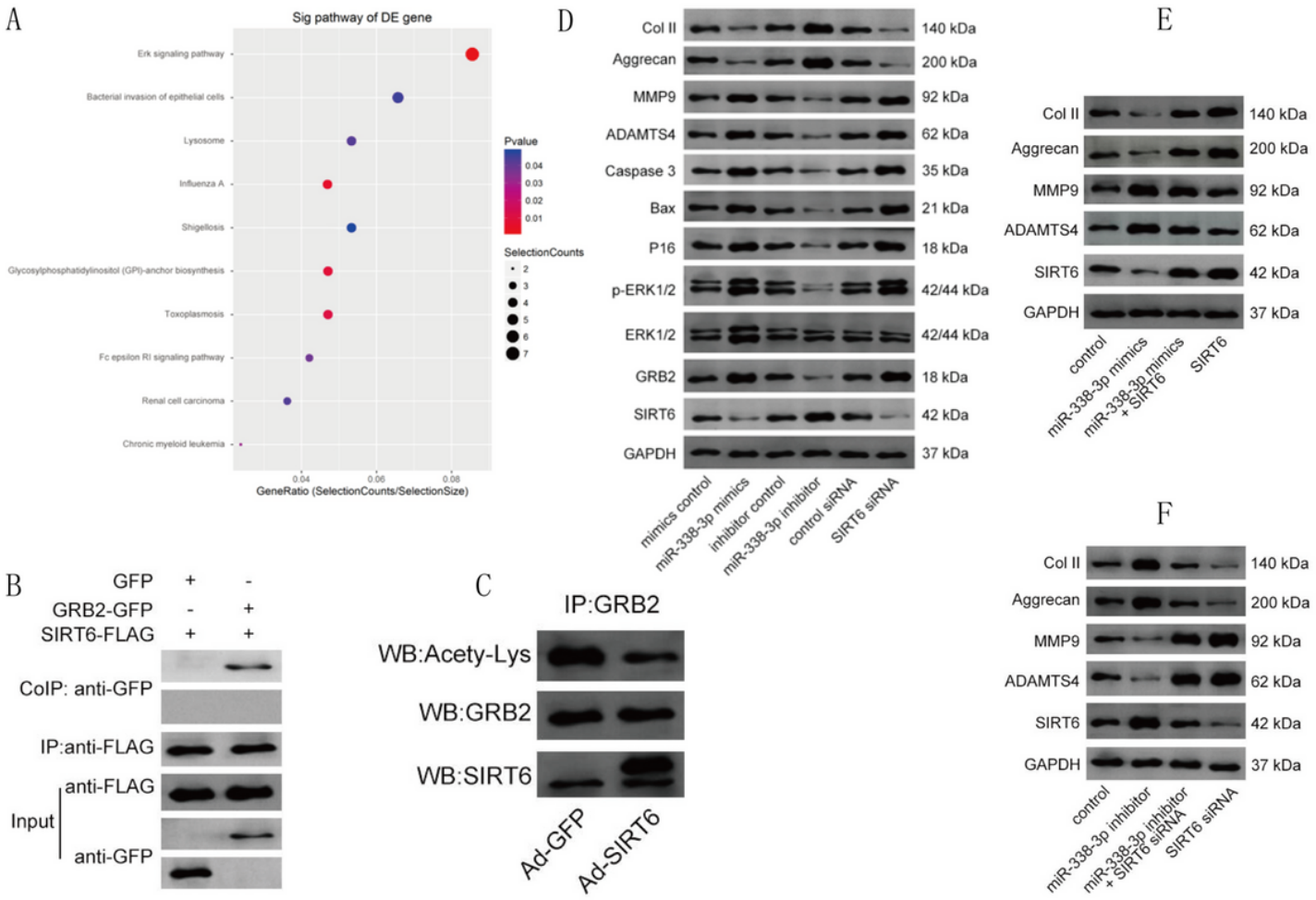

Figure 4

The modulation of miR-338-3p on SIRT6/MAPK/ERK signaling pathway. (A) KEGG analysis showing MAPK/ERK signaling pathway among the top-ranked pathways enriched with miRNAs downregulated in IDD samples. (B, C) Co-immunoprecipitation showing interactions between SIRT6 and GRB2. The deacetylated of GRB2 by SIRT6 resulting in its increased expression. (D)The expression levels of the proteins SIRT6, GRB2, ERK1/2, p-ERK1/2, P16, Bax, Caspase, Col II, Aggrecan, MMP9, and ADAMTS4 in human NP cells treated with miR-338-3p mimics/inhibitor and their negative controls siRNA, or SIRT6 siRNA. (E) The transfection of miR-338-3p mimics resulted in decreased expression levels of Col II and Aggrecan, whereas restoration of SIRT6 expression reversed this effect. Similarly, SIRT6 overexpression inhibited MMP9 and ADAMTS4 expressions, whereas miR-338-3p mimics reversed this decrease. (F) miR-338-3p inhibitor increased Col II and Aggrecan expressions, whereas silencing of SIRT6 stopped this effect. Similarly, SIRT6 knockdown increased MMP9 and ADAMTS4 expressions, whereas miR-338-3p inhibitor prevented this increase.

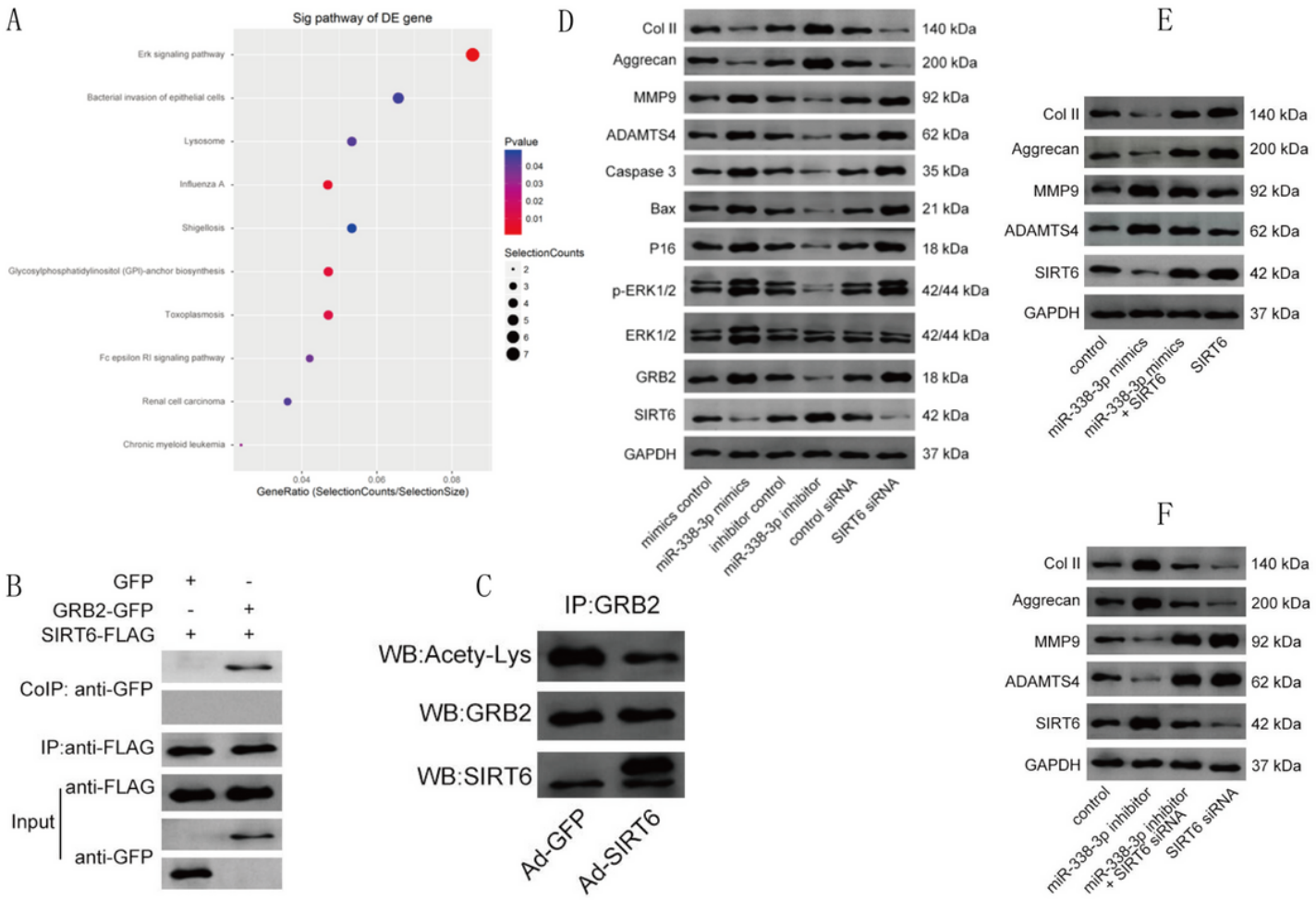

Figure 4

The modulation of miR-338-3p on SIRT6/MAPK/ERK signaling pathway. (A) KEGG analysis showing MAPK/ERK signaling pathway among the top-ranked pathways enriched with miRNAs downregulated in IDD samples. (B, C) Co-immunoprecipitation showing interactions between SIRT6 and GRB2. The deacetylated of GRB2 by SIRT6 resulting in its increased expression. (D)The expression levels of the proteins SIRT6, GRB2, ERK1/2, p-ERK1/2, P16, Bax, Caspase, Col II, Aggrecan, MMP9, and ADAMTS4 in human NP cells treated with miR-338-3p mimics/inhibitor and their negative controls siRNA, or SIRT6 siRNA. (E) The transfection of miR-338-3p mimics resulted in decreased expression levels of Col II and Aggrecan, whereas restoration of SIRT6 expression reversed this effect. Similarly, SIRT6 overexpression inhibited MMP9 and ADAMTS4 expressions, whereas miR-338-3p mimics reversed this decrease. (F) miR-338-3p inhibitor increased Col II and Aggrecan expressions, whereas silencing of SIRT6 stopped this effect. Similarly, SIRT6 knockdown increased MMP9 and ADAMTS4 expressions, whereas miR-338-3p inhibitor prevented this increase.

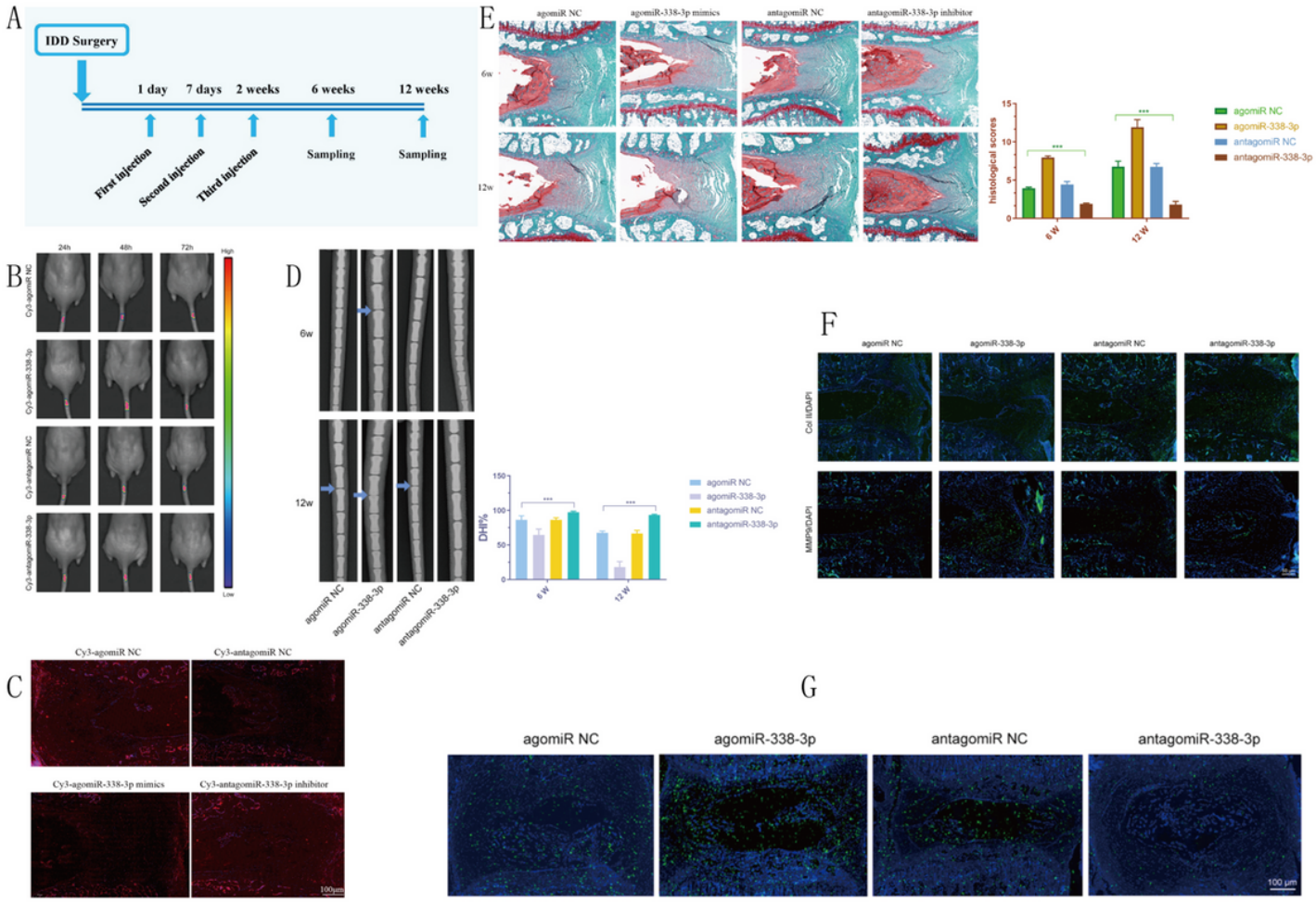

Figure 5

The therapeutic potential of miR-338-3p in IDD (A) Schematic diagram of the experimental design: intra-discal delivery of miR-338-3p mimics, mimics control, miR-338-3p inhibitor or control in mice models at 1st, 7th, and 14th days post IDD surgery. (B, C) In vivo fluorescence imaging at 24, 48 and 72 h post intra-discal injection of Cy3-antagomir-338-3p, Cy3-agomir-338-3p, or their negative controls (Scale bar = 100 μm) (D, E) The evaluation of the severity of IDD via the radiographical and histological findings on 6th and 12th weeks post IDD surgery. The intervertebral discs of mice treated with antagomir-338-3p show a significantly improved DHI% and histological score. (Scale bar = 50 μm). (F) Immunostaining showing the expression of Col II and MMP9 in mice models treated with ago- and antagomir-338-3p at 12th weeks post IDD surgery. (Scale bar = 100 μm) (G) TUNEL staining showing the degree of apoptotic activity in intervertebral discs of IDD model treated with ago- and antagomir-338-3p at the 12 weeks. (Scale bar = 100 μm) ***$p < 0.01$

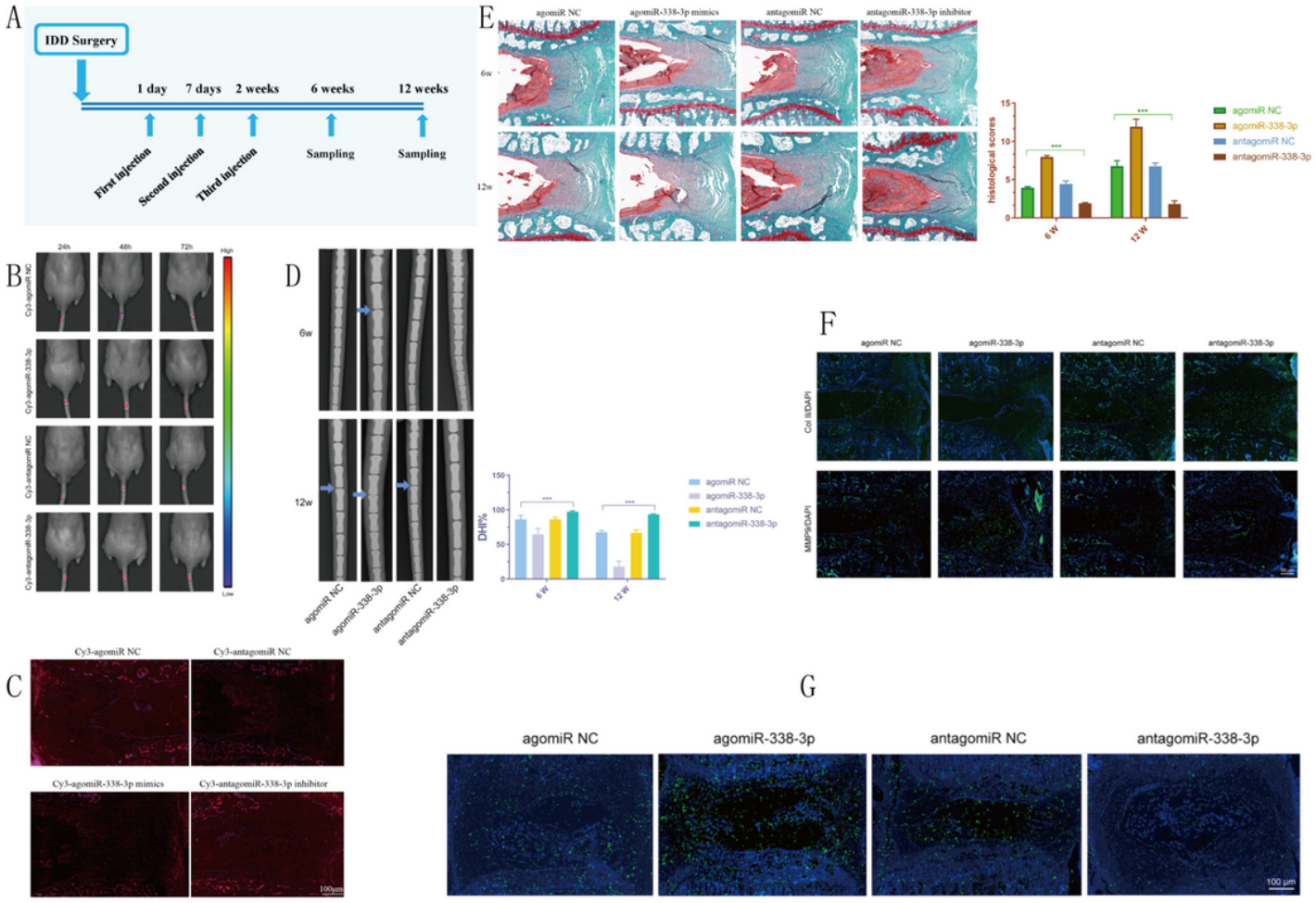

Figure 5

The therapeutic potential of miR-338-3p in IDD (A) Schematic diagram of the experimental design: intra-discal delivery of miR-338-3p mimics, mimics control, miR-338-3p inhibitor or control in mice models at 1st, 7th, and 14th days post IDD surgery. (B, C) In vivo fluorescence imaging at 24, 48 and 72 h post intra-discal injection of Cy3-antagomir-338-3p, Cy3-agomir-338-3p, or their negative controls (Scale bar = 100 μm) (D, E) The evaluation of the severity of IDD via the radiographical and histological findings on 6th and 12th weeks post IDD surgery. The intervertebral discs of mice treated with antagomir-338-3p show a significantly improved DHI% and histological score. (Scale bar = 50 μm). (F) Immunostaining showing the expression of Col II and MMP9 in mice models treated with ago- and antagomir-338-3p at 12th weeks post IDD surgery. (Scale bar = 100 μm) (G) TUNEL staining showing the degree of apoptotic activity in intervertebral discs of IDD model treated with ago- and antagomir-338-3p at the 12 weeks. (Scale bar = 100 μm) ***$p < 0.01$

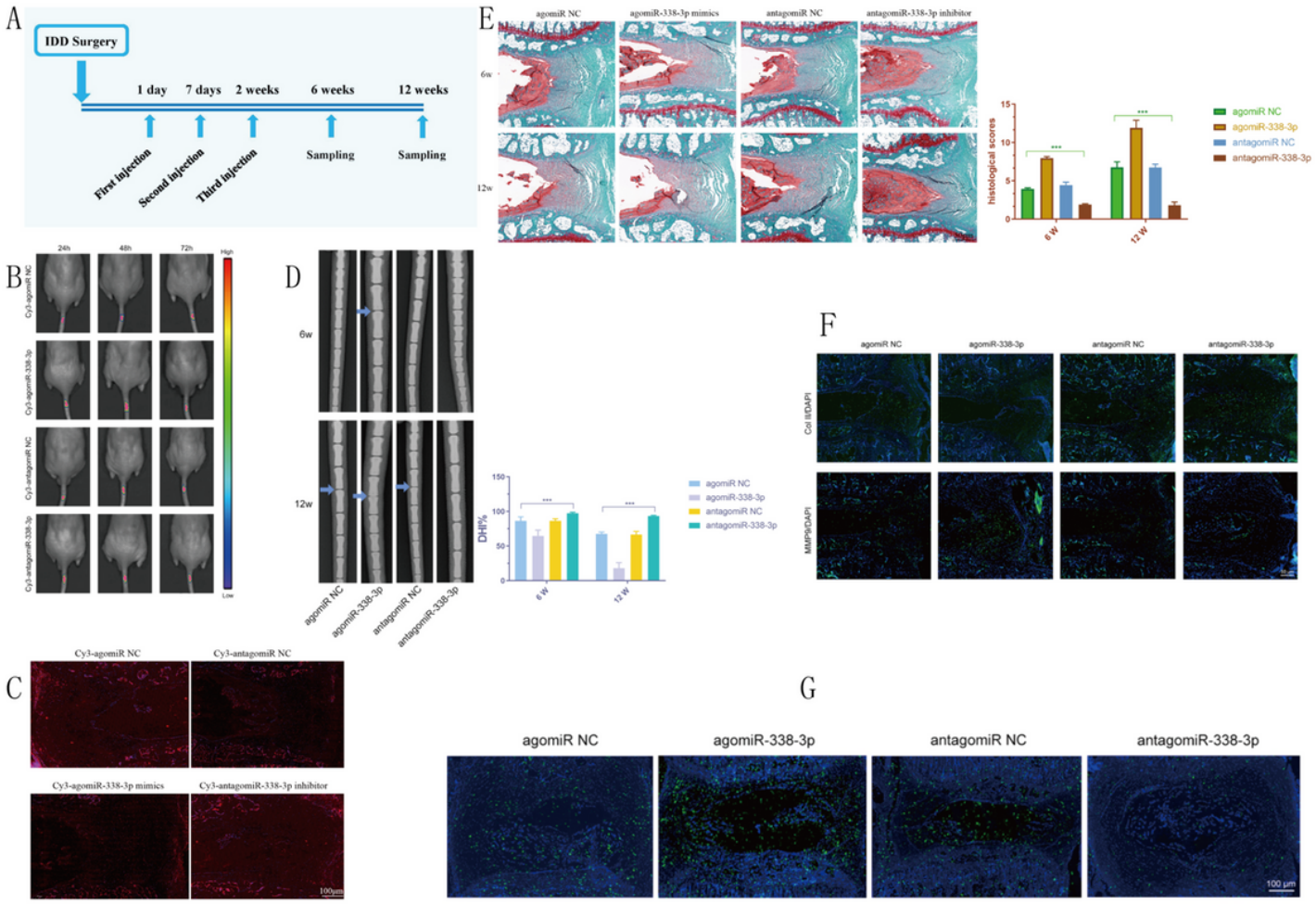

Figure 5

The therapeutic potential of miR-338-3p in IDD (A) Schematic diagram of the experimental design: intra-discal delivery of miR-338-3p mimics, mimics control, miR-338-3p inhibitor or control in mice models at 1st, 7th, and 14th days post IDD surgery. (B, C) In vivo fluorescence imaging at 24, 48 and 72 h post intra-discal injection of Cy3-antagomir-338-3p, Cy3-agomir-338-3p, or their negative controls (Scale bar = 100 μm) (D, E) The evaluation of the severity of IDD via the radiographical and histological findings on 6th and 12th weeks post IDD surgery. The intervertebral discs of mice treated with antagomir-338-3p show a significantly improved DHI% and histological score. (Scale bar = 50 μm). (F) Immunostaining showing the expression of Col II and MMP9 in mice models treated with ago- and antagomir-338-3p at 12th weeks post IDD surgery. (Scale bar = 100 μm) (G) TUNEL staining showing the degree of apoptotic activity in intervertebral discs of IDD model treated with ago- and antagomir-338-3p at the 12 weeks. (Scale bar = 100 μm) ***$p < 0.01$

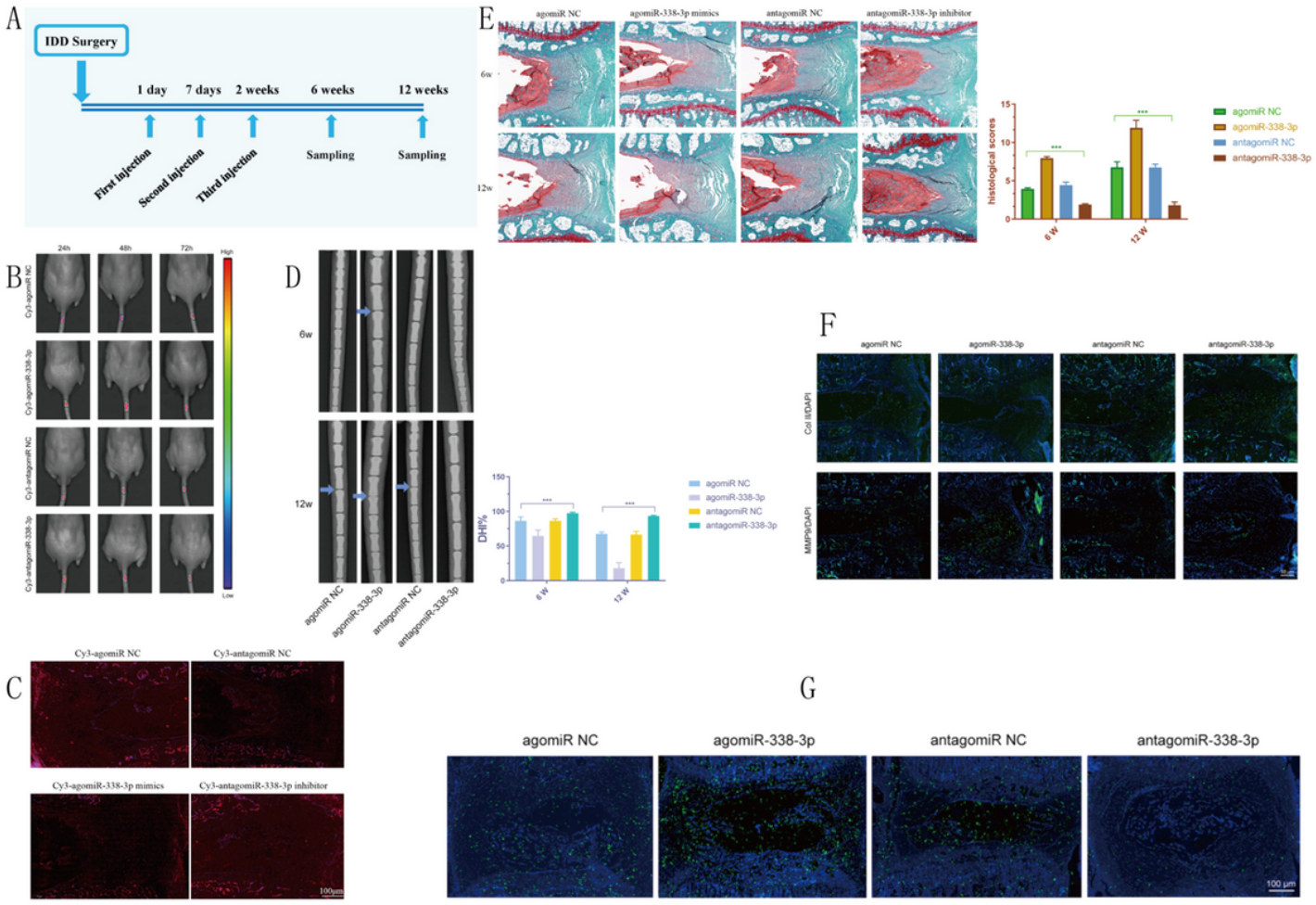

Figure 5

The therapeutic potential of miR-338-3p in IDD (A) Schematic diagram of the experimental design: intra-discal delivery of miR-338-3p mimics, mimics control, miR-338-3p inhibitor or control in mice models at 1st, 7th, and 14th days post IDD surgery. (B, C) In vivo fluorescence imaging at 24, 48 and 72 h post intra-discal injection of Cy3-antagomir-338-3p, Cy3-agomir-338-3p, or their negative controls (Scale bar = 100 μm) (D, E) The evaluation of the severity of IDD via the radiographical and histological findings on 6th and 12th weeks post IDD surgery. The intervertebral discs of mice treated with antagomir-338-3p show a significantly improved DHI% and histological score. (Scale bar = 50 μm). (F) Immunostaining showing the expression of Col II and MMP9 in mice models treated with ago- and antagomir-338-3p at 12th weeks post IDD surgery. (Scale bar = 100 μm) (G) TUNEL staining showing the degree of apoptotic activity in intervertebral discs of IDD model treated with ago- and antagomir-338-3p at the 12 weeks. (Scale bar = 100 μm) ***$p < 0.01$

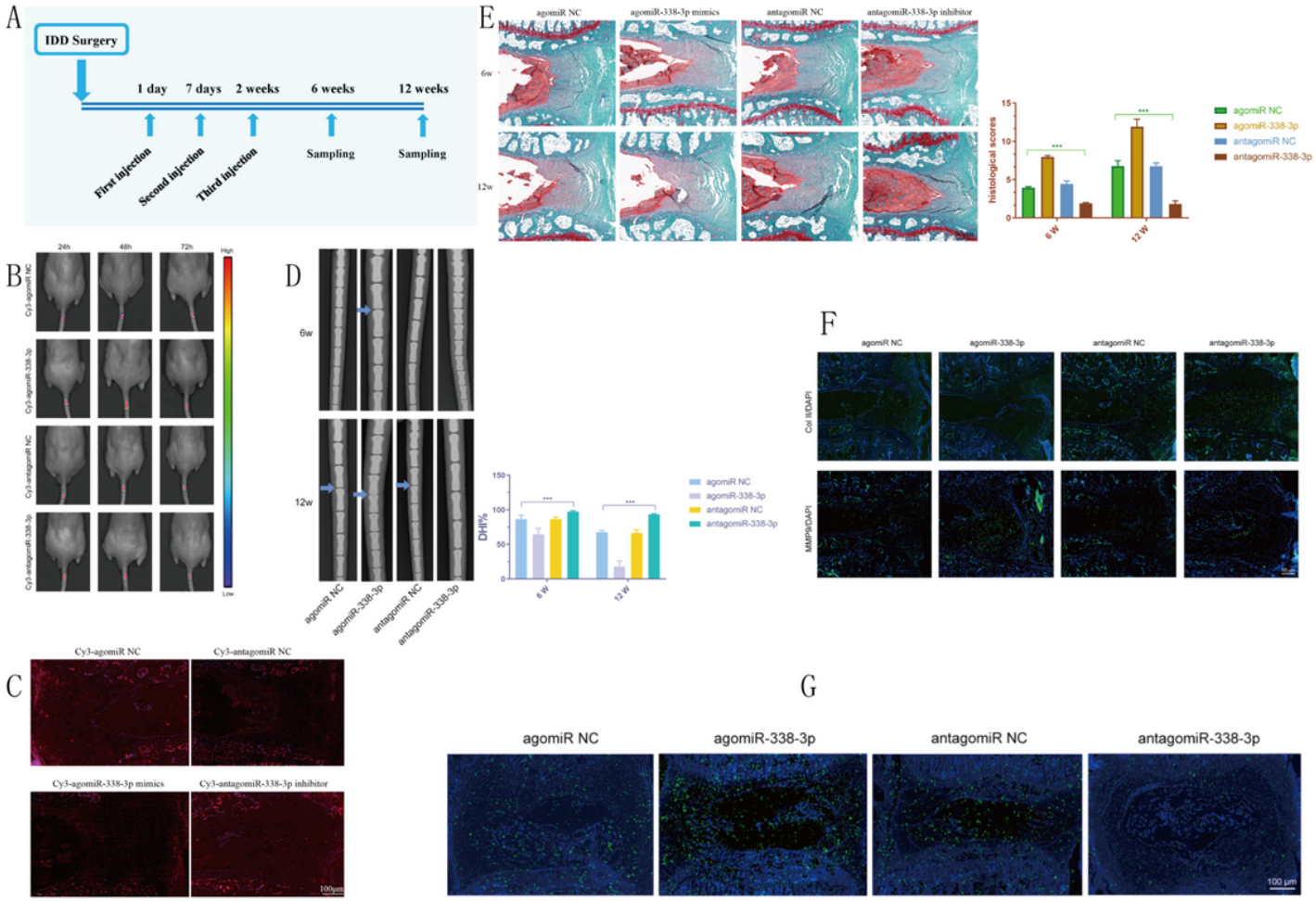

Figure 5

The therapeutic potential of miR-338-3p in IDD (A) Schematic diagram of the experimental design: intra-discal delivery of miR-338-3p mimics, mimics control, miR-338-3p inhibitor or control in mice models at 1st, 7th, and 14th days post IDD surgery. (B, C) In vivo fluorescence imaging at 24, 48 and 72 h post intra-discal injection of Cy3-antagomir-338-3p, Cy3-agomir-338-3p, or their negative controls (Scale bar = 100 μm) (D, E) The evaluation of the severity of IDD via the radiographical and histological findings on 6th and 12th weeks post IDD surgery. The intervertebral discs of mice treated with antagomir-338-3p show a significantly improved DHI% and histological score. (Scale bar = 50 μm). (F) Immunostaining showing the expression of Col II and MMP9 in mice models treated with ago- and antagomir-338-3p at 12th weeks post IDD surgery. (Scale bar = 100 μm) (G) TUNEL staining showing the degree of apoptotic activity in intervertebral discs of IDD model treated with ago- and antagomir-338-3p at the 12 weeks. (Scale bar = 100 μm) ***p < 0.01

Supplementary Files

This is a list of supplementary files associated with this preprint. Click to download.

- SupplementaryMaterial.pdf
- SupplementaryMaterial.pdf
- SupplementaryMaterial.pdf
- SupplementaryMaterial.pdf
- SupplementaryMaterial.pdf